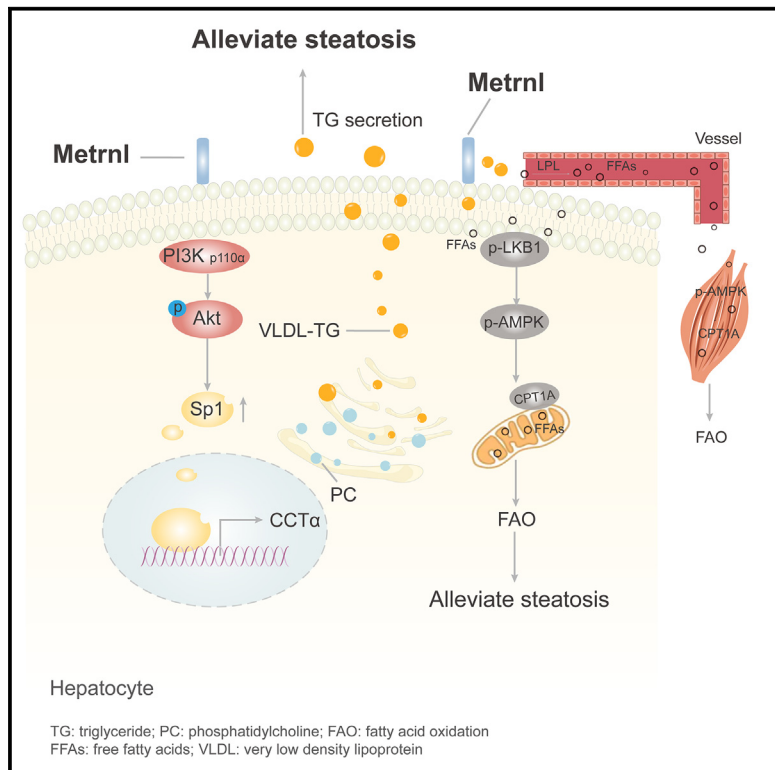


Meteorin-like alleviates hepatic steatosis by regulating hepatic triglyceride secretion and fatty acid oxidation

Graphical abstract



Authors

Lingyu Song, Yali Huang, Lu Liu, ..., Mingjun Shi, Yuxia Zhou, Bing Guo

Correspondence

smjtyf@126.com (M.S.),
zhouyuxia_27@163.com (Y.Z.),
guobingbs@126.com (B.G.)

In brief

Triglyceride (TG) secretion from the liver is critical in NAFLD progression and liver physiology, but the mechanism is not entirely clear. Song et al. show that Metrnl increases hepatic phosphatidylcholine synthesis to promote TG secretion and enhances fatty acid oxidation, suggesting an important role of Metrnl in liver lipid metabolism.

Highlights

- Metrnl plays a protective role in hepatic steatosis *in vivo*
- Metrnl is involved in hepatocyte TG secretion and fatty acid oxidation
- Increasing PC synthesis and AMPK activation were able to rescue hepatic steatosis



Article

Meteorin-like alleviates hepatic steatosis by regulating hepatic triglyceride secretion and fatty acid oxidation

Lingyu Song,^{1,6} Yali Huang,^{1,6} Lu Liu,¹ Xuebing Chang,¹ Laying Hu,¹ Guifang Wang,¹ Lifen Xu,⁴ Tian Zhang,¹ Yuanyuan Wang,¹ Ying Xiao,¹ Hong Yang,¹ Suye Ran,¹ Qing Shi,¹ Tuanlao Wang,⁵ Mingjun Shi,^{1,*} Yuxia Zhou,^{1,*} and Bing Guo^{1,2,3,7,*}

¹Department of Pathophysiology, and Department of Gastroenterology of the Affiliated Hospital of Guizhou Medical University, Guizhou Medical University, Gui'an New Area, 561113, China

²Guizhou Provincial Key Laboratory of Pathogenesis and Drug Research on Common Chronic Diseases and Guizhou Province Talent Base of Research on the Pathogenesis and Drug Prevention and Treatment for Common Major Diseases, Guizhou Medical University, Gui'an New Area, 561113, China

³Collaborative Innovation Center for Prevention and Control of Endemic and Ethnic Regional Diseases Co-constructed by the Province and Ministry, Guizhou Medical University, Gui'an New Area, 561113, Guizhou, China

⁴Department of Pathology, Affiliated Hospital of Guizhou Medical University, Guiyang, 550004, Guizhou, China

⁵School of Pharmaceutical Sciences, State Key Laboratory of Cellular Stress Biology, Fujian Provincial Key Laboratory of Innovative Drug Target Research, Xiamen University, Xiamen, 361005, Fujian, China

⁶These authors contributed equally

⁷Lead contact

*Correspondence: smjtyf@126.com (M.S.), zhouyuxia_27@163.com (Y.Z.), guobingbs@126.com (B.G.)

<https://doi.org/10.1016/j.celrep.2025.115246>

SUMMARY

Amid a rising prevalence of non-alcoholic fatty liver disease (NAFLD), there is still an unmet need to better treat it. We identified a secreted factor, Meteorin-like (Metrnl), with decreased levels in livers with hepatic steatosis. Notably, recombinant Metrnl ameliorated hepatic steatosis in NAFLD mouse models. Mechanistically, Metrnl exerted dual effects by promoting triglyceride (TG) transportation by the phosphatidylinositol 3-kinase (PI3K)/Akt/Sp1/cytidyltransferase α (CCT α) axis, thereby increasing the biosynthesis of phosphatidylcholine (PC) to facilitate TG secretion from the liver while facilitating AMP-activated protein kinase (AMPK)-dependent fatty acid oxidation (FAO). Exogenous injection of cytidine diphosphocholine (CDP)-choline, the production of CCT α , to increase PC synthesis, was shown to restore the inhibition of TG secretion in hepatic Metrnl-deficient (LKO-Met) mice. Combining CDP-choline and an AMPK activator was sufficient to rescue hepatic steatosis in LKO-Met mice. Collectively, these findings reveal unexpected roles of Metrnl as a factor in PC biosynthesis, TG secretion, and FAO, suggesting potential therapeutic application for NAFLD.

INTRODUCTION

Nonalcoholic fatty liver disease (NAFLD) is a clinicopathological syndrome that encompasses a pathophysiological spectrum of liver diseases ranging from simple steatosis to steatohepatitis and fibrosis. It is characterized by the presence of cardiometabolic risk factors such as obesity, type 2 diabetes, hypertension, and dyslipidemia. NAFLD has emerged as the most prevalent chronic liver disease, affecting approximately 25% of the global population. Nevertheless, few drugs are currently available to treat NAFLD.

The liver plays a crucial role in maintaining lipid homeostasis,¹ and abnormalities in hepatic lipid metabolism lead to the progression of NAFLD.² The excessive accumulation of triglycerides (TGs) in the liver is considered the initial stage of NAFLD pathology. Hepatic steatosis, caused by TG accumulation, is a promi-

nent feature of NAFLD and contributes to the development of nonalcoholic steatohepatitis, fibrosis, and cirrhosis.³ Hepatic steatosis ensues when TG export from the liver (such as decreasing TG secretion) fails to compensate for TG sources (such as increasing lipid uptake and lipogenesis and reducing free fatty acid (FFA) oxidation).⁴ However, the mechanism remains poorly understood. The liver alleviates TG accumulation by transporting TGs in the form of very-low-density lipoproteins (VLDLs), which primarily consist of TGs, phospholipids (such as phosphatidylcholine [PC]) and cholesterol. However, this rescue mechanism reaches a plateau when the TG content in the liver exceeds approximately 10%.⁵ Impaired assembly and secretion of VLDLs from the liver are important causes that exacerbate TG accumulation in the liver.^{4,6} Conversely, increasing TG secretion in the VLDL fraction has been identified as an effective therapeutic approach to address hepatic TG accumulation.^{6,7} However,



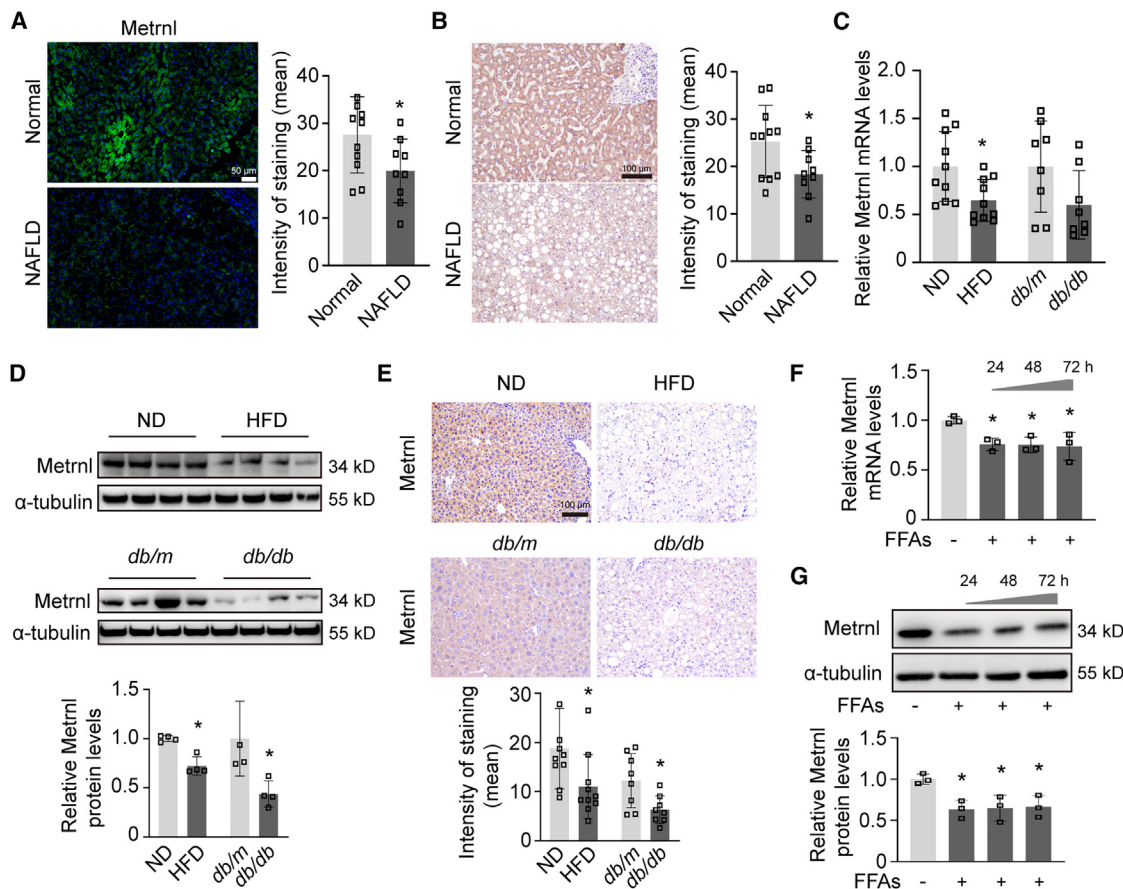


Figure 1. Metrnl expression levels are decreased in the fatty livers of patients and mice and in FFA-treated HepG2 cells

(A and B) Representative fluorescence images of Metrnl mRNA levels determined by fluorescence *in situ* hybridization (A; scale bar, 20 μ m) and protein levels detected by IHC (B; scale bar, 100 μ m) in the livers of healthy controls and patients with NAFLD ($n = 9-11$). (C–E) The hepatic Metrnl mRNA (C) and protein (D and E) levels in mouse models with NAFLD (HFD-fed and *db/db*) were detected by qPCR, WB, and IHC, respectively ($n = 4-10$). The HFD and MCD groups were fed for 16 and 8 weeks, respectively. Scale bar, 100 μ m. (F and G) The mRNA (F) and protein (G) expression of Metrnl in HepG2 cells treated with (0.3 mmol/L) or without FFAs at the indicated time points ($n = 3$). The data are presented as the mean \pm SD. * $p < 0.05$ and ** $p < 0.01$ compared with the respective controls.

increasing TG export from the liver is often associated with side effects, such as elevated circulating TG levels and cholesterol levels in the blood, both of which are critical factors associated with cardiovascular risk,⁸ which restricts the development of efficient treatment strategies targeting TG export from the liver to treat NAFLD.

Here, we show that the secretory protein Meteorin-like (Metrnl) has a novel effect on TG secretion from the liver without obvious side effects as a treatment for NAFLD. Metrnl is a secretory protein that is highly expressed in muscle, adipose, and barrier tissues^{9,10} and has been found to exert many metabolic benefits, such as increasing fatty acid oxidation (FAO) in skeletal muscle,⁹ promoting adipocyte differentiation,¹¹ enhancing beige-fat thermogenesis,¹² and improving insulin resistance.^{9,11} However, the role of Metrnl in hepatic lipid homeostasis remains poorly understood. Our findings indicate that Metrnl effectively alleviates hepatic steatosis through pharmacological interventions in mouse NAFLD models. Furthermore, Metrnl promotes TG secretion from the liver while avoid-

ing adverse effects during NAFLD treatment. We also found that Metrnl increases hepatic PC biosynthesis to regulate TG secretion while simultaneously increasing the capacity of liver and muscle tissues to consume FFAs (hydrolysate from circulating TGs) by promoting FAO. These results provide new insights into metabolic control while also providing new therapeutic strategies for the treatment of hepatic lipid-associated disorders.

RESULTS

Metrnl expression is decreased in fatty livers of patients and mice

Immunohistochemical (IHC) staining revealed that Metrnl is ubiquitously expressed in human tissues and is more highly expressed in the liver than in the other 10 types of human tissues (Figure S1A). We investigated the potential role of Metrnl in NAFLD by measuring the mRNA and protein levels of Metrnl in liver tissue arrays from individuals with NAFLD, NAFLD model

mice (HFD-fed and *db/db* mice), and FFA-treated HepG2 cells. As presented in Figures 1A and 1B, the Metrnl mRNA and protein levels were significantly reduced in the livers of individuals with NAFLD and in HFD-fed and *db/db* mice compared to their respective controls (Figures 1C–1E and S1B). Furthermore, the expression levels of Metrnl in HepG2 cells decreased after 24, 48, and 72 h of incubation with FFAs (Figures 1F and 1G).

Based on gene expression patterns from the single nucleus RNA sequencing data (GSE223558), a total of 5 clusters of cells were generated, and hepatocytes composed the largest group (76%) (Figure S1C). We analyzed Metrnl expression in various mouse liver cell types and found that it was abundant, including in hepatocytes (Figure S1D). By performing an immunofluorescence colocalization analysis, we also observed that Metrnl was coexpressed with albumin (ALB), a specific biomarker of hepatocytes (Figure S1E).

We investigated the relationship between Metrnl expression and NAFLD progression by analyzing the intensity of IHC staining for Metrnl in relation to the area of steatosis. The expression levels of Metrnl in humans, HFD-fed mice, and *db/db* mice tended to negatively correlate with steatotic areas, especially in the livers of HFD-fed mice (Figures S2A–S3C). These results suggest that Metrnl may play a role in hepatic steatosis and that its expression might be linked to metabolic changes in the mouse and human liver.

Recombinant Metrnl ameliorates hepatic steatosis in mice with NAFLD

We produced the recombinant Metrnl protein (rMet), verified it via SDS-PAGE, and confirmed its identity using Coomassie blue staining and western blotting (WB) to confirm its role in hepatic lipid metabolism (Figure S3A). We subsequently investigated the effect of rMet on *db/db* mice and found that it reduced the hepatic TG content, steatosis, and staining for F4/80, a macrophage biomarker, compared to control mice (Figure S3C). Additionally, the rMet group presented lower body weights, liver weights, alanine aminotransferase (ALT) levels, aspartate aminotransferase (AST) levels, fasting blood glucose (FBG) levels, and inflammatory cell infiltration in the liver than the control group (Figures S3D–S3H and S3J); however, no significant change in the serum TG content was observed following rMet treatment (Figure S3I).

Next, we administered rMet to C57BL/6J mice, which were also fed an HFD for 16 weeks (Figure S4A). Compared with those in the HFD group, the HFD-induced increases in hepatic TG content, steatosis, and F4/80 expression were significantly reduced following rMet treatment (Figures S4B and S4C). Additionally, the body weight, liver weight, FBG level, area of steatosis, and ALT level were decreased upon rMet treatment (Figures S4D–S4H and S4J), whereas no significant changes in the serum TG content were detected upon rMet treatment (Figure S4I). The mice were fed an HFD for 16 weeks, resulting in remarkable hepatic steatosis, followed by therapeutic administration of rMet for 8 weeks to investigate the therapeutic effect of rMet on NAFLD development (Figure 2A). No significant differences in food intake were observed between the HFD-fed and HFD-fed rMet-treated mice (Figure S5A). However, hepatic TG accumulation, steatosis, and F4/80 expression were alleviated in the livers

of the rMet-treated HFD-fed mice compared with those of the control mice (Figures 2B and 2C). Similarly, the body weights of the rMet-treated mice decreased after 16 weeks of HFD challenge (Figure 2D), primarily due to loss of liver mass and reduction in weight of visceral adipose tissue (Figure S5B). Moreover, compared with HFD feeding, rMet treatment led to decreased liver weight, FBG levels, steatotic area, inflammatory cell infiltration, and ALT and AST levels (Figures 2E–2H and 2J). Furthermore, a trend toward decreased serum TG content was observed following rMet treatment (Figure 2I). In terms of metabolic impairment, insulin resistance is a hallmark of hepatic steatosis. We detected insulin resistance in HFD-fed mice, and the areas under the curves for both the intraperitoneal glucose tolerance test and the intraperitoneal insulin tolerance test revealed that insulin resistance was improved in HFD-fed rMet-treated mice compared with control HFD-fed mice (Figures S5C and S5D). Taken together, these findings suggest that rMet alleviates hepatic steatosis in mouse models with NAFLD via both preventative and therapeutic administration. Moreover, we constructed adeno-associated virus 8 (AAV8), which carries mouse Metrnl, to overexpress Metrnl in *db/db* mice (Figure S6A). Similarly, AAV8-mediated Metrnl overexpression ameliorated hepatic steatosis in *db/db* mice (Figures S6B–S6J).

Metrnl increases hepatic PC content and TG secretion

Then, we utilized untargeted absolute quantitative lipidomics to assess the lipid composition in the livers of HFD-fed mice (Figure 3A). Similar to the results presented in Figures S3, S4C, and 2C, the analysis of lipid classes revealed significant decreases in TG levels in HFD-fed mice after rMet treatment (Figure 3B). Additionally, we observed reduced levels of TG species, as depicted in Figure 3C. Notably, treatment with rMet noticeably increased the hepatic levels of several glycerol phosphatides, including the phosphatidylserine, phosphatidylinositol, phosphatidylethanolamine (PE), PC, and phosphatidic acid classes (Figure 3B).

TGs are exported from the liver in the form of VLDL particles. Phospholipid synthesis plays a crucial role in the biogenesis and secretion of VLDL,¹³ with PC being an essential component of VLDL. The results revealed a significant increase in PC levels in the rMet treatment group (Figures 3B and 3D). Consistent with these findings, we observed elevated PC content in the livers of rMet-treated HFD-fed mice and *db/db* mice compared with their respective controls (Figures 3E and S3K). We directly evaluated the rates of TG secretion *in vivo* by intraperitoneally injecting mice with poloxamer 407, an inhibitor of lipoprotein lipase (LPL) that can prevent TG uptake from other tissues so that the rate of TG secretion can be determined in the blood.¹⁴ As expected, rMet significantly increased TG secretion in both HFD-fed and *db/db* mice (Figures 3F and S3L). In addition, fast protein liquid chromatography revealed elevated VLDL levels in the serum of rMet-treated HFD-fed mice as well as relatively increased low-density lipoprotein (LDL) and high-density lipoprotein (HDL) levels (Figure 3G). We also measured TG secretion *in vitro* to further clarify that the induction of VLDL-TG secretion in HFD-fed and *db/db* mice was specific to hepatocytes and not influenced by factors outside the liver. As shown in Figure 3H, Metrnl protein levels were notably increased by Ad-Met and

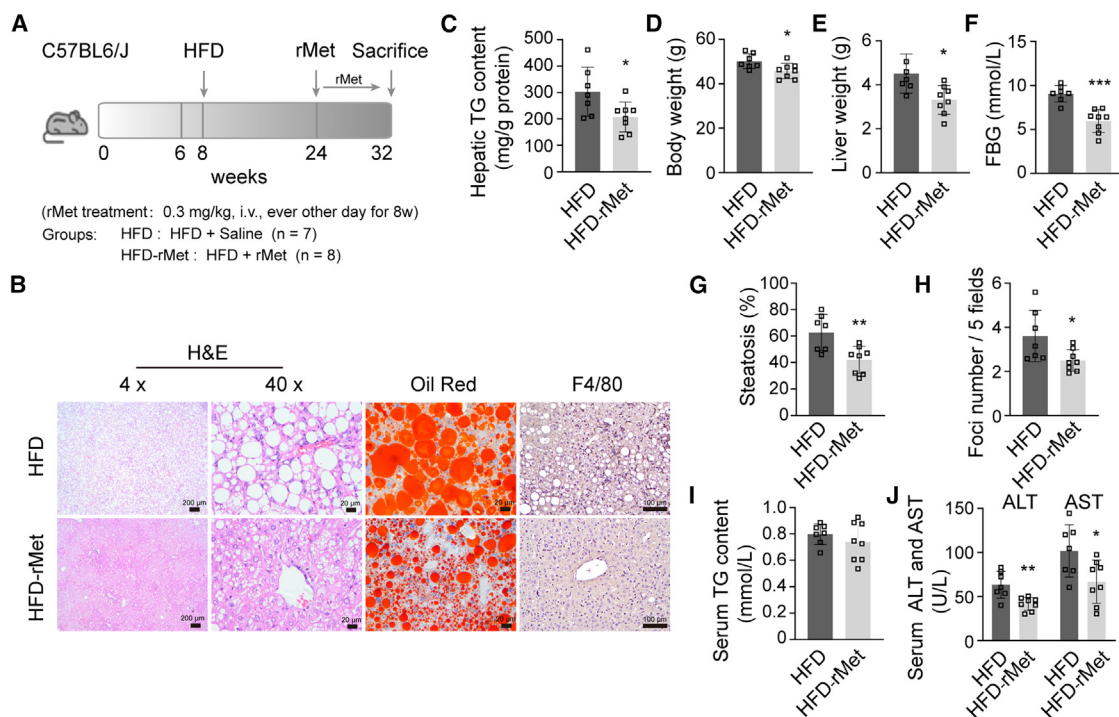


Figure 2. The therapeutic administration of rMet attenuates TG accumulation in HFD-fed mice

(A) Experimental procedure for the HFD-fed mice. At age 8 weeks, C57BL/6 mice were fed an HFD for 16 weeks and subsequently administered rMet through a tail vein injection (0.3 mg/kg every other day) and fed an HFD for 8 weeks ($n = 7-8$).
(B) Images of H&E, oil red O, and F4/80 staining of liver samples from HFD-fed and HFD-fed rMet-treated mice. Scale bars, 200 or 20 μ m
(C–J) The hepatic TG content (C), body weight (D), liver weight (E), FBG level (F), area of steatosis (G), number of foci from H&E staining (H), plasma TG content (I), and ALT and AST levels (J) were determined in HFD-fed and HFD-fed rMet-treated mice.
rMet, recombinant Metrl; TG, triglyceride; LW, liver weight; BW, body weight; FBG, fasting blood glucose; ALT, alanine transaminase; AST, glutamic oxaloacetic transaminase. The data are presented as the mean \pm SD. * $p < 0.05$ and ** $p < 0.001$ compared with the HFD-fed group.

decreased by adenovirus-mediated expression of shRNA-Metrl (sh-Met 1, sh-Met 2, and sh-Met 3) in HepG2 cells, and sh-Met 1 was used for subsequent studies because of its relatively high knockdown efficiency. We detected a decrease in the intracellular TG concentration and an increase in the TG content in the supernatant, along with an increase in PC content, in the FFA-treated HepG2 cells after Ad-Met treatment compared with cells in the Ad-Veg group (Figures 3I and 3J). Conversely, the intracellular TG concentration increased, whereas the PC content and extracellular TG concentration decreased, in the FFA-treated HepG2 cells after sh-Met treatment (Figures 3K–3L).

We conducted experiments using primary hepatocytes to further investigate the effect of Metrl on TG secretion. We generated mice with Metrl deletion in hepatocytes (Metrl^{flox/flox}, ALB^{Cre+}, LKO-Met) and matched control mice (Metrl^{flox/flox}, ALB^{Cre-}, L-WT) (Figure 3M). Primary hepatocytes were isolated from both L-WT and LKO-Met mice, and the knockout efficiency was confirmed by qPCR (Figure 3N). These isolated hepatocytes were then incubated with FFAs for 24 h, and then the intracellular and supernatant TG contents were measured. The results revealed elevated intracellular TG content and decreased TG content in the supernatant, along with a reduction in intracellular PC content, in hepatocytes from LKO-Met mice compared with those from L-WT mice, and these

changes in the primary hepatocytes of LKO-Met mice were reversed after exogenous rMet treatment (Figures 3O and 3P). Importantly, the ¹³C-labeled PC levels were also increased after Ad-Met or rMet treatment in AML12 cells and primary hepatocytes from LKO-Met and L-WT mice (Figures 3Q–3S), indicating that the number of newly synthesized PCs was increased by Metrl. In a choline- and methionine-deficient diet-induced NAFLD mouse model, which features choline deficiency, causing TG secretion disorders that lead to hepatic steatosis, we did not observe any alleviation of hepatic steatosis after rMet treatment (Figures S7A–S7F). These results indicate that the reduction in intracellular TG content in the rMet-treated mice may be partly attributed to the increases in PC content and TG secretion.

Metrl regulates PC biosynthesis and TG secretion through the Sp1/CCT α axis

The liver is essential for PC production via the Kennedy pathway (Figure 4A) and the methylation of PE, which is catalyzed by PE N-methyltransferase (PEMT). These two processes account for two-thirds and one-third of PC synthesis, respectively.¹⁵ Following the increase in PC content in hepatocytes after Metrl treatment, we analyzed the expression of PC synthesis enzymes in HepG2 cells exposed to FFAs. Our findings revealed that

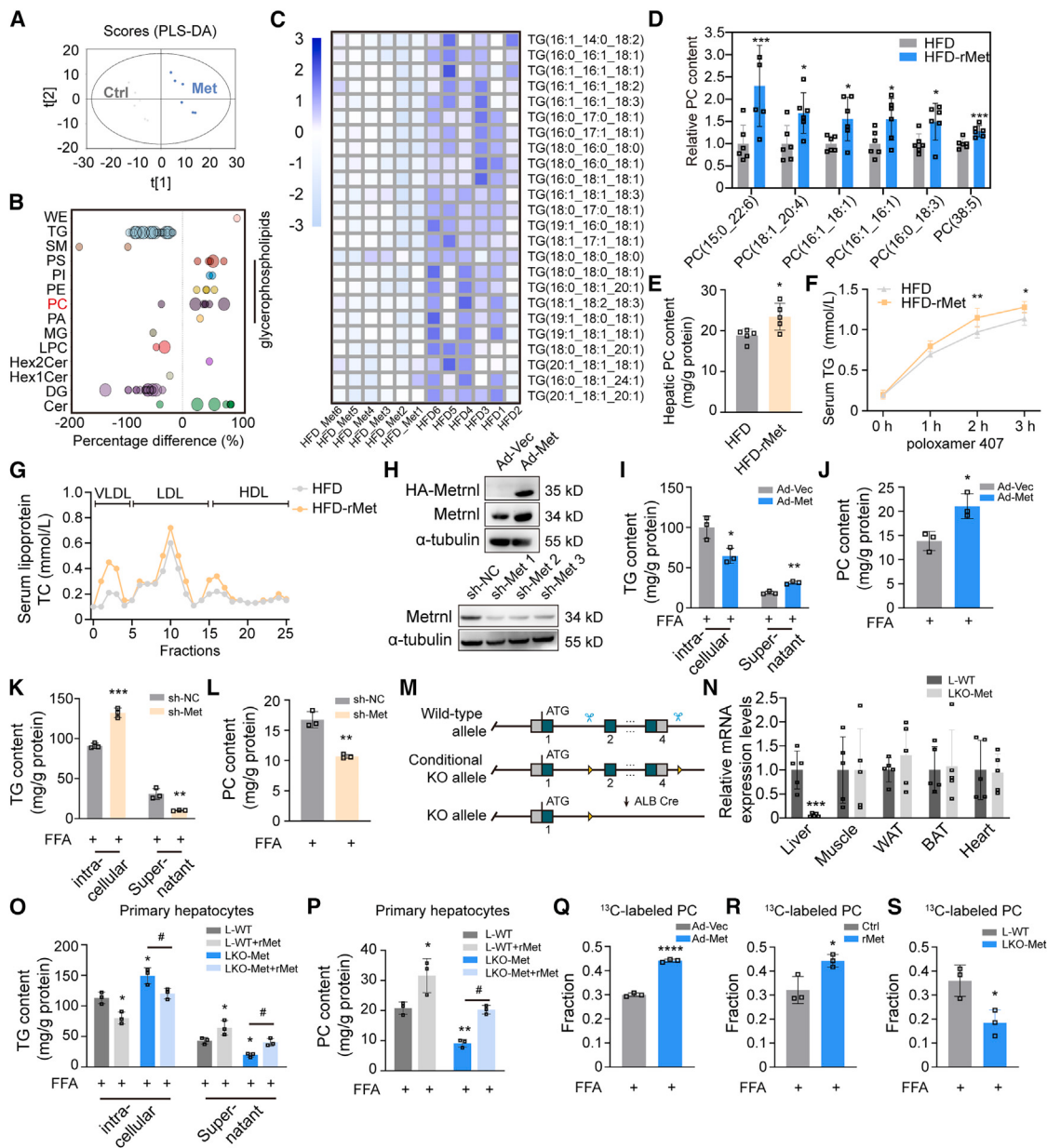


Figure 3. Metrnl increases the hepatic PC content and TG secretion

(A–D) Lipidomics analyses of hepatic lipid classes (B), hepatic TG species (C), and PC species (D) in HFD-fed mice treated with or without rMet ($n = 6$). (E) The hepatic PC content was determined in HFD-fed mice ($n = 5$).

(F) TG secretion rates were detected in the serum of HFD-fed mice after TG uptake by extrahepatic tissues was blocked through an intraperitoneal injection of poloxamer 407 (1 mg/g body weight) at the indicated time points (0, 1, 2, and 3 h) ($n = 5$).

(G) Contents of circulating VLDL, LDL, and HDL particles in HFD-fed mice ($n = 5$).

(H) Immunoblots showing the levels of the indicated proteins in HepG2 cells 48 h after the adenovirus injection ($n = 3$).

(I and K) Intracellular and supernatant TC contents of FFA-treated HepG2 cells after Ad-Vec, Ad-Met (H), Ad-sh-NC (sh-NC), or Ad-sh-Met (sh-Met) (J) treatment ($n = 3$).

(J and L) PC content in FFA-treated HepG2 cells after Ad-Vec, Ad-Met (I), sh-NC, or sh-Met (K) treatment ($n = 3$).

(M) Strategy for generating the liver-specific Metrnl-KO mouse (LKO-Met) strain using CRISPR-Cas9 technology.

(N) Identification of the specific knockout of Metrnl in the livers of Met-LKO mice by qPCR.

(O and P) Intracellular and supernatant TG contents (O) and intracellular PC contents (P) of primary hepatocytes isolated from L-WT and LKO-Met mice incubated with FFAs (0.3 mmol/L) and with or without rMet (100 ng/mL) for 24 h ($n = 5$).

(legend continued on next page)

Metrnl increased the mRNA and protein levels of cytidyltransferase α (CCT α) but did not significantly affect the levels of choline kinase alpha, choline/ethanolamine phosphotransferase, or PEMT (Figures 4B and 4C). Consistent with these results, we also observed increased levels of CCT α in AML12 cells (Figure 4D), primary hepatocytes from LOK-Met and L-WT mice (Figure 4E), and the livers of HFD-fed mice treated with rMet (Figures 4F and 4G). As CCT α is the rate-limiting enzyme involved in the Kennedy pathway, mice deficient in CCT α presented with decreased PC content accompanied by reduced VLDL secretion and TG accumulation in the liver.¹⁶ When liver-specific CCT α -deficient mice were fed an HFD for 10 weeks, they developed hepatic steatosis.¹⁷ Therefore, Metrnl may increase the levels of PC by upregulating CCT α .

The transcription factor Sp1 binds to the promoter of CCT α , and downregulation of Sp1 by a small interfering RNA inhibited CCT α promoter activity during S phase.¹⁸ We examined the expression of Sp1 in HepG2 cells and the livers of HFD-fed mice to investigate how Metrnl regulates CCT α expression. As shown in Figure 4C, the expression levels of Sp1 were increased by Ad-Met and reduced by sh-Met in both the total protein- and FFA-treated HepG2 cells. Similar results were observed in HFD-fed mice treated with rMet (Figures 4G and 4H). The Sp1 nucleoprotein was also positively regulated by Metrnl (Figure 4I). Next, we observed that Ad-Met markedly increased the expression levels of Sp1 and CCT α as well as the PC content and TG secretion, during FFA challenge; however, these effects were attenuated by the specific Sp1 inhibitor mithramycin A (Mith) (Figures 4J–4L). Additionally, we performed a dual-luciferase reporter assay by constructing a plasmid with the CCT α promoter (which contains the target sequence that interacts with Sp1) in HEK293T cells. The results revealed that the transcriptional activity of the CCT α promoter was greater in the Ad-Met-infected group than in the Ad-Vec-infected group (Figure 4M). In addition, the chromatin immunoprecipitation sequencing (ChIP)-qPCR results clearly demonstrated that Sp1 binds to the promoter region of CCT α , and this binding was notably increased by Metrnl overexpression in HepG2 cells (Figure 4N). In conclusion, our results indicate that the Sp1/CCT α axis plays a crucial role in the Metrnl-mediated increases in PC biosynthesis and TG secretion upon high fat exposure.

Metrnl activates Sp1/CCT α -mediated PC biosynthesis and TG secretion through the PI3K p110 α /Akt pathway

We studied the signaling pathways Metrnl influences, specifically the p38 mitogen-activated protein kinase, peroxisome proliferator-activated receptor γ , phosphatidylinositol 3-kinase (PI3K)/Akt, and STAT3 pathways, as noted in prior research, to examine its effects on Sp1 activation.^{10,19} Our results revealed that Ad-Met significantly increased p-Akt levels, whereas sh-Met decreased its levels (Figure 5A), and Metrnl had little effect on other pathways. Activation of the PI3K/Akt pathway increases Sp1 expression.^{20,21} We verified that Metrnl regulates p-Akt

levels in AML12 cells via rMet treatment and that rMet treatment could reverse the reduction in p-Akt levels caused by Metrnl deficiency in primary hepatocytes (Figures 5B and 5C). Additionally, treatment with the PI3K inhibitor LY294002 partially reversed the Ad-Met-induced increases in the Sp1, CCT α , and PC contents and TG secretion in HepG2 cells (Figures 5D–5F). We performed an ELISA to measure the level of Metrnl in the supernatant of FFA-treated HepG2 cells and found that Metrnl overexpression increased its level, whereas Metrnl knockdown reduced it (Figure 5G). Additionally, blocking secreted Metrnl with a Metrnl-neutralizing antibody effectively reduced the increases in the p-Akt and PC levels and TG secretion induced by Ad-Met in FFA-treated HepG2 cells (Figures 5H–5J). These findings suggest that Metrnl leads to Akt activation, PC synthesis, and TG secretion, which depend on increased Metrnl secretion induced by Ad-Met.

HepG2 cells were cultured with rMet to further determine whether exogenous Metrnl can increase the level of p-Akt. The results showed that rMet dose-dependently increased p-Akt levels after 30 min of incubation, within the concentration range of 1–100 ng/mL (Figure 5K). Additionally, when HepG2 cells were pretreated with LY294002 (a broad-spectrum inhibitor of PI3K) and PIK75 (an inhibitor of the catalytic subunit of PI3K, p110 α), rMet-mediated Akt activation was nearly completely abolished (Figure 5L). However, inhibition of the p110 β catalytic subunit of PI3K with the specific inhibitor TGX221 did not blunt rMet-mediated Akt activation (Figure 5L). Taken together, these results indicate that Metrnl regulates PC biosynthesis and TG secretion through the PI3K p110 α /Akt/Sp1/CCT α axis.

Metrnl overexpression promotes FAO in an AMPK-dependent manner

We detected the expression levels of genes involved in TG metabolism to more comprehensively elucidate the underlying mechanism of Metrnl in hepatic TG metabolism (Figures 6A, S8A, and S8B). Our findings revealed that, in addition to ApoB, a gene associated with lipid transport, the key enzyme CPT1A, which is responsible for FAO, was significantly upregulated in HepG2 cells treated with Ad-Met (Figure 6A). The CPT1A protein level was also increased in FFA-treated HepG2 cells and AML12 cells and in the livers of HFD-fed mice after Ad-Met or rMet treatment (Figures 6B, 6C, and 6E) and was decreased in primary hepatocytes from LKO-Met mice (Figure 6D). Additionally, we measured the levels of ketone bodies and ATP, which are the byproducts of hepatic FAO.²² Our data suggested that the levels of β -hydroxybutyric acid and ATP were significantly increased in the liver tissues of HFD-fed mice treated with rMet and in the HepG2 cells treated with Ad-Met (Figures 6F, 6G, 6I, and 6J).

Previously, we reported that Metrnl maintains the palmitic acid-mediated decrease in mitochondrial dynamics via AMP-activated protein kinase (AMPK) activation.²³ AMPK is a crucial energy sensor that controls the metabolism of organs, and AMPK activation not only promotes the oxidative decomposition

(Q and R) 1,2-¹³C-labeled PC in AML12 cells after Ad-Met/Ad-Vec (Q) and rMet/Ctrl treatment for 48 h (R).

(S) 1,2-¹³C-labeled PC in primary hepatocytes from L-WT and LKO-Met mice.

L-WT, Metrnl ^{flox/flox}, ALB Cre $^{-}$ mice; LKO-Met, Metrnl ^{flox/flox}, ALB Cre $^{+}$ mice; WAT, white adipose tissue; BAT, brown adipose tissue. The data are presented as the mean \pm SD. * p < 0.05, ** p < 0.01, and *** p < 0.001 compared with the HFD, Ad-Vec, sh-NC, or L-WT groups. # p < 0.05 compared with the LKO-Met group.

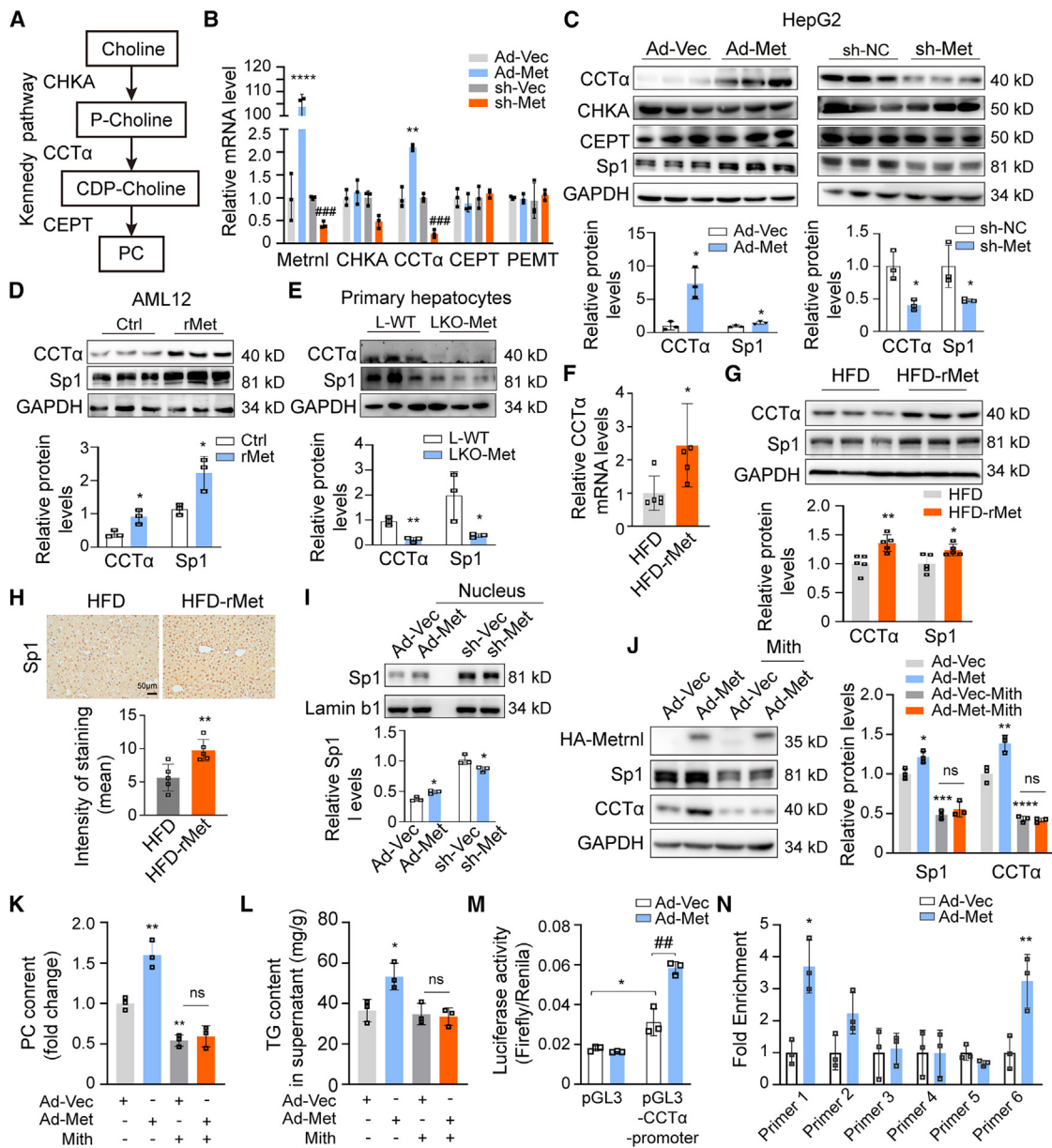


Figure 4. Metrnl regulates PC biosynthesis and TG secretion via the Sp1/CCT α axis

(A) The Kennedy pathway for PC biosynthesis.

(B and C) FFA-treated HepG2 cells were transfected with an adenovirus for 48 h, and the mRNA levels of the genes involved in PC biosynthesis (B) and the protein levels of Sp1 and the genes involved in PC biosynthesis (C).

(D and E) Protein levels in FFA-treated AML12 cells (D) and primary hepatocytes from LKO-Met mice and L-WT mice (E).

(F–H) The expression levels were measured in the livers of HFD-fed and HFD-rMet mice using qPCR (F), WB (G), and IHC (H) ($n = 5$).

(I) Sp1 expression was detected in the nuclear extracts of FFA-treated HepG2 cells 48 h after the adenovirus infection ($n = 3$).

(J–L) Sp1 and CCT α expression (J) and PC (K) and TG contents (L) were determined in FFA-treated HepG2 cells transfected with the adenovirus and incubated with 100 nmol/L Mith (an Sp1-specific inhibitor) for 24 h ($n = 3$).

(M) A dual-luciferase assay was performed in HEK293T cells 24 h after the transfection of a CCT α -promoter plasmid and adenovirus infection, and the empty plasmid pGL3 was used as a control ($n = 3$).

(N) qPCR analysis of the levels of the CCT α promoter enriched with an anti-Sp1 antibody or an immunoglobulin G (IgG) antibody via a ChIP assay in Metrnl-overexpressing or control HepG2 cells.

Mith, mithramycin. The data are presented as the mean \pm SD. * $p < 0.05$ and ** $p < 0.01$ compared with the Ad-Vec, sh-NC, or HFD groups.

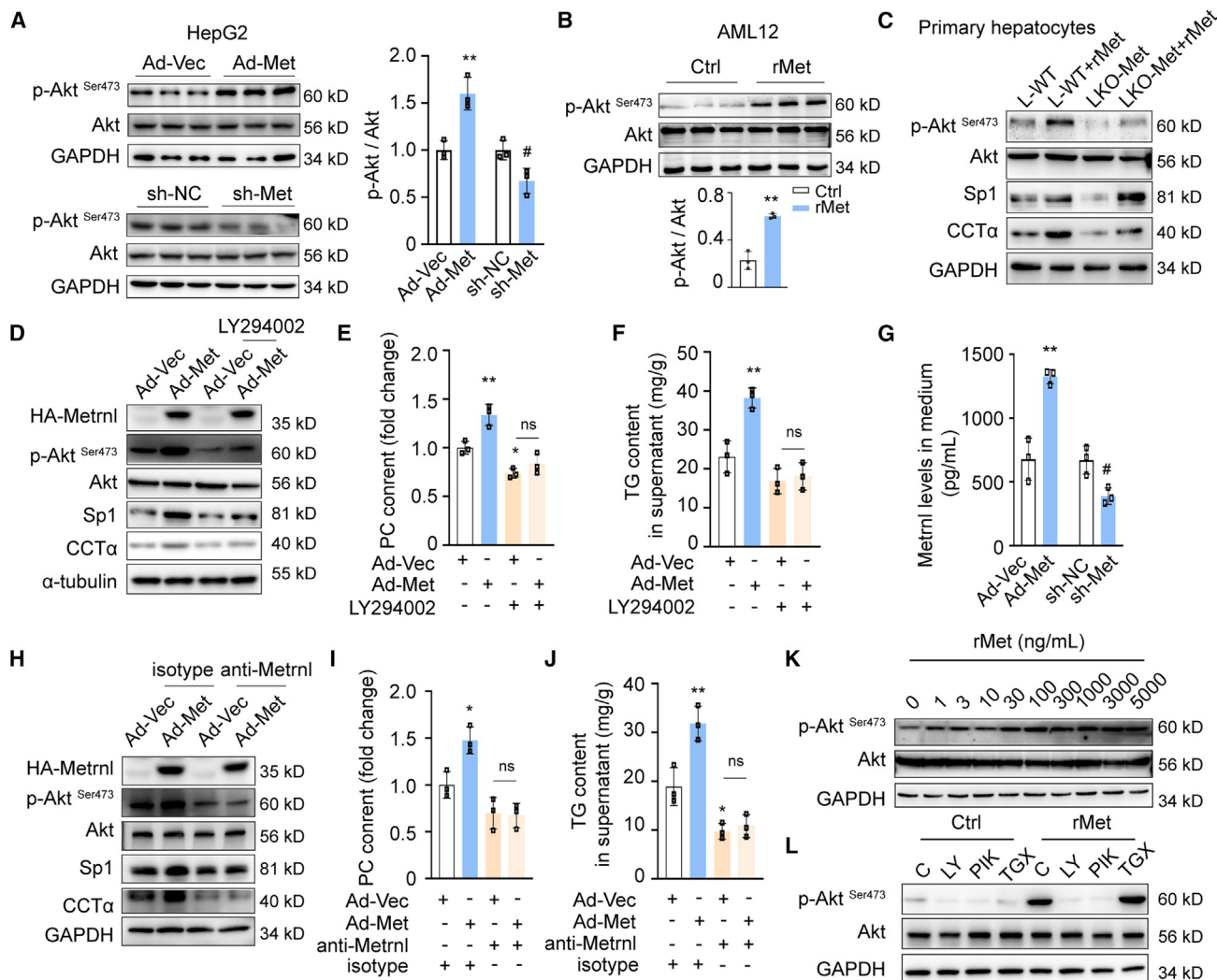


Figure 5. Metrnl activates Sp1/CCT α -mediated PC biosynthesis and TG secretion through the PI3K p110 α /Akt pathway

(A-C) The protein expression levels were measured using WB in FFA-treated HepG2 cells (A), AML12 cells (B), and primary hepatocytes isolated from L-WT and LKO-Met mice treated with rMet (100 ng/mL) (C) for 24 h or left untreated.

(D-F) The protein expression levels (D), PC content (E), and TG secretion in the supernatant (F) were determined in FFA-treated HepG2 cells incubated with or without LY294002 (10 μ M/L) and the adenovirus for 24 h.

(G-J) The Metrnl concentration in the medium was measured using ELISA (G), and Akt activity was confirmed by treating FFA-treated HepG2 cells with the Metrnl-neutralizing antibody (H) and measuring the PC content (I) and TG secretion in the medium (J) 24 h after the adenovirus infection. The isotype control antibody was used as a control antibody.

(K-L) Protein levels were determined after treatment with different doses of rMet (K) with or without LY294002 (LY), PIK75 (PIK) (100 μ M/L), TGX221 (TGX) (100 μ M/L), or rMet (100 ng/mL) for 30 min (L) ($n = 3$).

The data are presented as the mean \pm SD. * $p < 0.05$ and ** $p < 0.01$ compared with the Ad-Vec, sh-Vec, or Ctrl groups.

of lipids in the liver but also enhances the oxidative decomposition of muscle tissue.²⁴ In this study, we also found that the levels of p-AMPK were positively regulated by Ad-Met or rMet treatment (Figures 6B–6E) and that the ability of Metrnl to increase CPT1A expression, β -hydroxybutyric acid levels, and ATP content was attenuated by the AMPK inhibitor compound C (Com C) in HepG2 cells treated with FFAs (Figures 6H–6J). Considering the involvement of AMPK activation, we investigated three main kinases (p-LKB1, p-CaMKK2, and p-TAK1) that positively regulate AMPK activation. We showed that p-LKB1 levels were posi-

tively regulated by Metrnl in FFA-treated HepG2 cells, AML12 cells, and primary hepatocytes (Figures 6B–6D), and similar results were observed in the livers of HFD-rMet mice (Figure 6E). However, minimal differences in p-CaMKK2 and p-TAK1 levels were observed between the Ad-Met and Ad-Vec groups following FFA exposure (Figure 6B). Therefore, the increase in p-LKB1 levels is associated with the upregulation of AMPK mediated by Metrnl overexpression or rMet treatment. Because FAO is closely associated with cellular oxygen consumption, our results revealed that the oxygen consumption rate (OCR) was

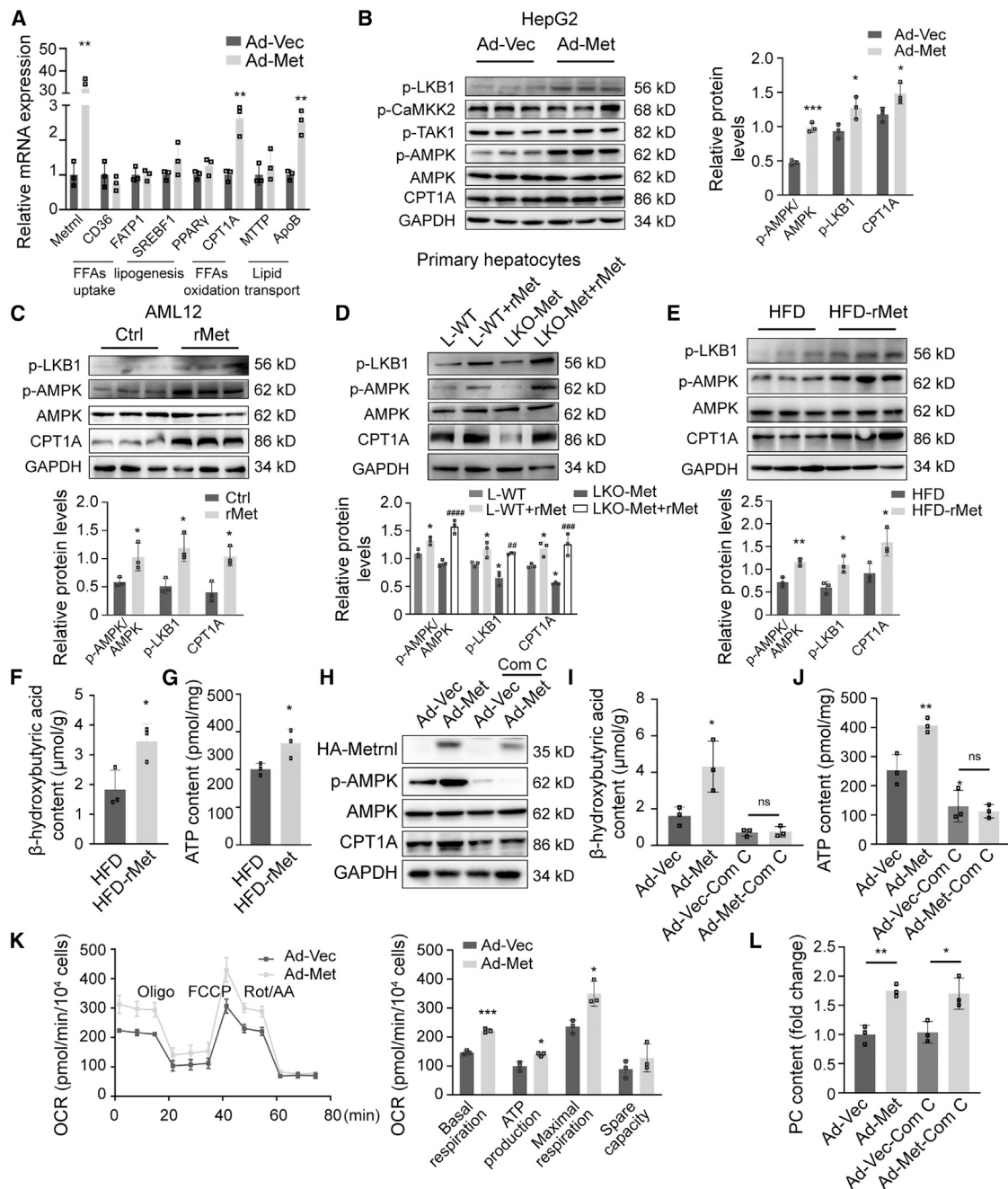


Figure 6. Metrnl overexpression promotes hepatic FAO in an AMPK-dependent manner

(A) The mRNA levels of genes involved in lipid metabolism in FFA-treated HepG2 cells ($n = 3$).

(B–E) WB analysis of the AMP-activated protein kinase (AMPK) pathway in FFA-treated HepG2 cells 24 h after the adenovirus infection (B), in AML12 cells 24 h after rMet (100 ng/mL) treatment (C), in primary hepatocytes from L-WT and LKO-Met mice treated with rMet (100 ng/mL) for 24 h or left untreated (D), and in the livers of HFD and HFD-rMet mice (E) ($n = 3–5$).

(F–G) Hepatic β-hydroxybutyric acid (F) and ATP contents (G) were detected in HFD-fed and HFD-fed rMet mice ($n = 5$).

(H–J) WB analysis (H) and measurement of the β-hydroxybutyric acid (I) and ATP contents (J) in FFA-treated HepG2 cells after adenovirus treatment with or without Com C challenge (10 μmol/L) for 24 h ($n = 3$).

(legend continued on next page)

significantly increased after Metrnl overexpression in FFA-treated HepG2 cells (Figure 6K). We analyzed PC levels in HepG2 cells treated with FFAs after Com C treatment to assess whether AMPK activation influences the Metrnl-induced increase in hepatic PC content and found that the increase in PC levels induced by Ad-Met was not significantly affected by Com C (Figure 6L).

Hepatocytes secrete TG into the bloodstream, where it is then hydrolyzed into FFAs. These FFAs in the circulation are taken up by adjacent tissues. The process of TG hydrolysis in circulation is catalyzed by LPL.²⁵ Additionally, we found that the serum LPL activity in HFD-rMet mice was increased (Figure S9A). These findings suggest that Metrnl has a stimulatory effect on TG hydrolysis. However, the serum FFA content decreased in HFD-fed mice after rMet treatment (Figure S9B), indicating that more FFAs were taken up by adjacent tissues.

Given that FAO in skeletal muscle is also related to hepatic steatosis,²² the effect of rMet on FAO in the skeletal muscle tissues of HFD-fed mice was examined. Consistent with the increased FAO in the liver, the levels of CPT1A, p-AMPK, and ATP content in the skeletal muscle tissues of HFD-fed mice, and the OCR in a mouse skeletal muscle cell line (C2C12) tended to increase upon rMet administration (Figures S9C–S9F). Collectively, these results indicate that Metrnl enhances FAO in an AMPK-dependent manner in both the liver and skeletal muscle and helps to consume excess serum FFAs resulting from TG hydrolysis catalyzed by LPL.

The restoration of PC biosynthesis and AMPK activation are sufficient to rescue hepatic steatosis induced by hepatic Metrnl deficiency in HFD-fed mice

We further investigated the relationships among hepatic Metrnl, PC synthesis, and steatosis progression by conducting an experiment using LKO-Met and L-WT mice. Both groups were fed an HFD for 14 weeks, followed by an intraperitoneal injection of cytidine diphosphocholine (CDP)-choline for 2 weeks at the end of the HFD challenge (Figure 7A). As expected, we observed a decrease in the serum TG levels after poloxamer 407 administration as well as a decrease in the serum TG content and hepatic PC content in LKO-Met mice compared with those in L-WT mice fed an HFD (Figures 7B–7D). Previous studies have shown that the inhibition of TG secretion caused by CCT α knockout can be reversed via exogenous CDP-choline treatment.¹⁶ We hypothesized that restoring PC synthesis by CDP-choline administration would ameliorate the impaired TG secretion caused by hepatic Metrnl deficiency. We found that the levels of secreted TGs in the serum of LKO-Met mice were significantly lower than those in the serum of L-WT mice after the injection of poloxamer 407; however, CDP-choline treatment was sufficient to restore the impaired TG secretion in LKO-Met mice (Figure 7B), reversing the decreases in the serum TG content and hepatic PC

content induced by hepatic Metrnl deficiency (Figures 7C and 7D).

Moreover, compared with L-WT mice, LKO-Met mice exhibited increased hepatic steatosis and hepatic TG accumulation when subjected to an HFD. However, the hepatic TG content and steatosis induced by hepatic Metrnl deficiency in the livers of mice injected with CDP-choline were alleviated (Figures 7E and 7F). Additionally, CDP-choline and acadesine (AICAR), an AMPK activator, effectively rescued the hepatic TG content and steatosis induced by Metrnl deficiency in the liver in mice fed an HFD (Figures 7E and 7F). No obvious differences in food intake, body weight, FBG levels, or fasting blood insulin levels were observed between L-WT and LKO-Met mice treated with CDP-choline and AICAR or left untreated, but the liver weight was elevated in LKO-Met mice compared with L-WT mice and was significantly decreased after CDP-choline and AICAR treatment (Figures S10A–S10E). These findings suggest that the absence of Metrnl in the liver exacerbates hepatic steatosis and TG accumulation by reducing CDP-choline-mediated PC synthesis and TG secretion while suppressing AMPK-mediated FAO.

DISCUSSION

NAFLD is the most common chronic liver disease, but therapeutic regimens targeting NAFLD remain unmet needs. In this study, we elucidated a previously unrecognized role of Metrnl in regulating hepatic TG secretion and increasing FAO. These findings suggest that Metrnl could be a promising therapeutic target for NAFLD and related metabolic diseases. Mechanistically, we showed that Metrnl activates the PI3K/Akt pathway, leading to increased Sp1-mediated CCT α transcription. Thus, increased PC synthesis could promote TG secretion from the liver but did not exacerbate the TG, FFA, or cholesterol burdens in the blood. Additionally, Metrnl activates the LKB1/AMPK signaling pathway to promote FAO in the liver and skeletal muscle.

PC is an essential molecule that regulates the normal physiological function of the body, including VLDL assembly and secretion.²⁶ The livers of individuals with simple steatosis and patients with NASH show a decrease in PC content.²⁷ CCT α , the key enzyme in the Kennedy pathway of PC synthesis, plays a critical role in TG secretion. CCT α mutation has been identified in patients with fatty liver disease,²⁸ and CCT α deficiency leads to hepatic steatosis and reduced VLDL secretion.¹⁶ The administration of exogenous CDP-choline, the catalytic product of CCT α , effectively restores PC biosynthesis caused by the loss of mTORC1 activity.⁶ These findings indicate a close relationship between CCT α -mediated PC biosynthesis and NAFLD progression. However, the regulation of CCT α expression is not fully understood. Although the transcription factor Sp1 is associated

(K) Analysis of oxygen consumption in FFA-treated HepG2 cells 48 h after Metrnl overexpression or transfection of the control plasmid. These cells were then sequentially exposed to oligomycin (Oligo), carbonyl cyanide-p-trifluoromethoxyphenylhydrazone (FCCP), and rotenone/antimycin A (Rot/AA) to determine different parameters, which were detected using a Seahorse analysis ($n = 3$).

(L) The PC content was detected in FFA-treated HepG2 cells 24 h after adenovirus infection with or without compound C (Com C) challenge (10 μ mol/L) ($n = 3$). The data are presented as the mean \pm SD. * $p < 0.05$ and ** $p < 0.01$ compared with the Ad-Vec, Ctrl, L-WT, or HFD group. # $p < 0.05$ and ** $p < 0.01$ compared with LKO-Met mice.

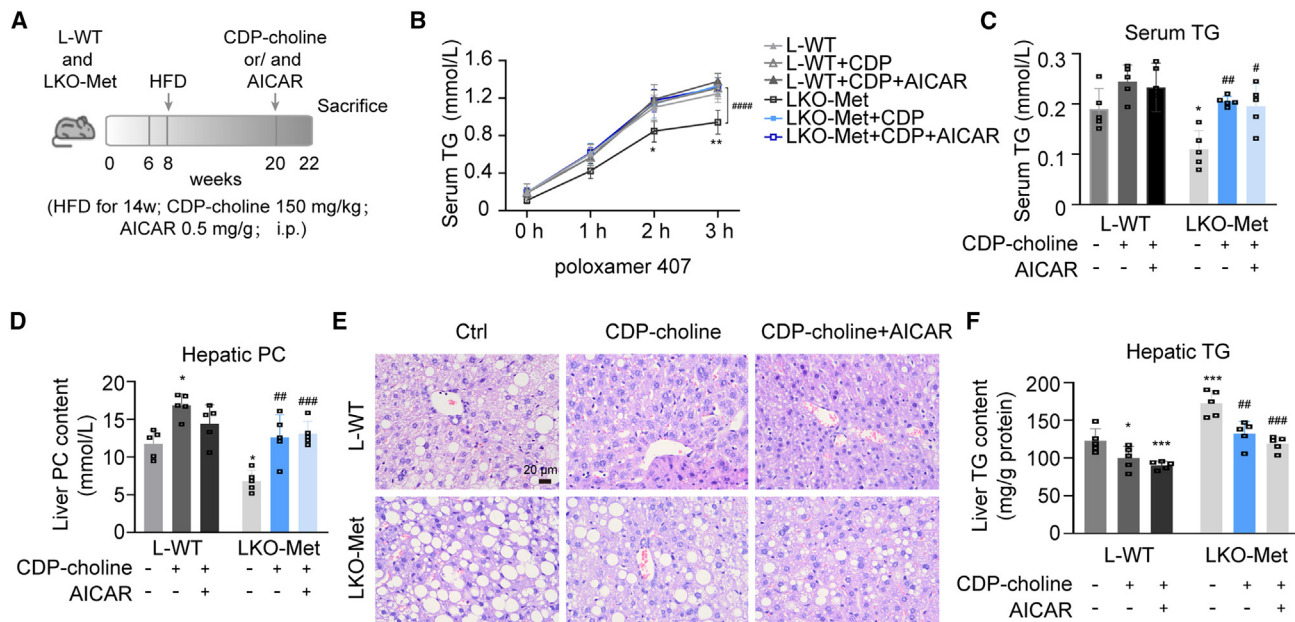


Figure 7. The restoration of PC biosynthesis and AMPK activation are sufficient to rescue hepatic TG accumulation in LKO-Met mice fed an HFD

(A) Six-week-old LKO-Met and L-WT mice were fed an HFD for 12 weeks. In the last 2 weeks, the mice were injected with saline, CDP-choline (150 mg/kg), or AICAR (0.5 mg/g) for 2 weeks ($n = 5$).

(B–F) TG secretion in the serum after fasting for 4 h and subsequent poloxamer 407 treatment (B), serum TG content (C), hepatic PC content (D), H&E staining (E), and the hepatic TG content (F) were determined.

L-WT, Metrnl^{flox/flox}, ALB Cre⁻ mice; LKO-Met, Metrnl^{flox/flox}, ALB Cre⁺ mice; CDP, CDP-choline; AICAR, acadesine, an AMPK activator. The data are presented as the mean \pm SD. * $p < 0.01$ and ** $p < 0.001$ compared with L-WT mice; # $p < 0.05$, ## $p < 0.01$, and ##### $p < 0.0001$ for the comparison of LKO-Met+CDP-choline mice and LKO-Met mice.

with sphingolipid metabolism,²⁹ which is also a major component of phospholipids, its effect on glycerophospholipid metabolism, including PC synthesis, remains unknown. In this study, we observed that Metrnl acts as an important regulator of CCT α expression, PC synthesis, and TG secretion. Metrnl upregulates Sp1 expression to facilitate hepatic lipid export, which is a crucial physiological process for systemic lipid transport to extrahepatic tissues *in vivo*.⁶

Previous reports have shown that activation of the PI3K/Akt pathway plays a critical role in regulating lipid metabolism in both humans and mice.³⁰ Adenovirus-mediated hepatic expression of constitutively active Akt results in elevated VLDL levels in Western diet-fed *L1^{B6}Ldlr^{-/-}* and *Ldlr^{-/-}* mice.³¹ Furthermore, various studies have shown that Metrnl can increase p-Akt levels in different cell types.¹⁹ Consistent with these findings, our study further elucidated the potential role of Metrnl in regulating TG secretion induced by the PI3K/Akt pathway, indicating its critical biological function in lipid homeostasis *in vivo*. Although Akt has been shown to increase hepatic lipogenesis,³² increased p-Akt levels in the liver are associated with the amelioration of steatosis in diabetic mice,³³ indicating that the regulatory effect of Akt on hepatic lipid homeostasis is complicated. In addition, the increased FAO and ATP contents in the muscle of rMet-treated HFD-fed mice may partially offset or even exceed the increase in lipogenesis induced by Akt activation. Additionally, we further showed that the Metrnl-mediated increase in p-Akt levels occurs

via a PI3K p110 α -dependent pathway in liver cells, which is consistent with the finding that p110 α predominantly mediates Akt activation in the liver,³⁴ where the selective inhibition of p110 α increases lipid deposition.³⁵

Based on the quantitative lipidomics data, rMet also decreased the diglyceride (DG) content in the livers of HFD-fed mice, which serves as both a precursor to PC and an intermediate product of TG synthesis. A previous study reported that PC synthesis requires the consumption of DG, and this process is also controlled by the Kennedy pathway.³⁶ This result may explain why the lipidomics data revealed an obvious decrease in the DG content in the livers of the rMet-treated HFD-fed mice despite the lack of changes in the expression of genes involved in lipogenesis following Metrnl overexpression.

Given that VLDL particles contain TG and cholesterol, we measured the total serum cholesterol (TC) concentration *in vivo*. However, no significant difference in TC content in the serum was observed between HFD-fed and rMet-treated mice (Figure S10A). Since cholesterol in the blood can be transported back to the liver for bile acid synthesis by HDL, and since PC is also involved in HDL formation,²⁶ we examined the serum HDL concentration and found that it was higher in rMet-treated mice than in HFD-fed mice (Figure S11B). Another study also revealed that Metrnl-deficient mice present decreased blood HDL levels.³⁷ Taken together, these findings suggest that rMet promotes PC synthesis and TG secretion from the liver

without increasing the cholesterol burden of the cardiovascular system.

Furthermore, AMPK is a crucial metabolic energy sensor that enhances FAO.³⁸ Numerous studies have demonstrated that AMPK agonists can reduce the accumulation of TGs by promoting fatty acid β -oxidation. Consistent with previous research showing that Metrnl significantly increases the level of AMPK phosphorylation in skeletal muscle cells,⁹ we also observed increased AMPK phosphorylation in the skeletal muscle of rMet-treated HFD-fed mice. AMPK is primarily activated by kinases such as LKB1, CaMKK β , or TAK1.^{39–42} However, our study revealed that Metrnl increased the levels of only p-LKB1 and not p-CaMKK β or p-TAK1. This increase in p-LKB1 levels led to an increase in CPT1A expression, which further fueled β -oxidation and promoted FFA consumption. In a previous study, we reported that Metrnl-mediated AMPK activation in renal tubular epithelial cells depends on Sirt3,²³ which interacts with LKB1 and positively regulates LKB1 expression.⁶ However, further investigations are needed to determine how Metrnl promotes LKB1/AMPK-mediated FAO in muscle or other organs.

Moreover, increasing circulating Metrnl levels has been found to promote thermogenic effects on adipose tissue,¹² which may cause a decrease in body weight, a factor that could affect hepatic steatosis. Although some loss of body weight was observed in the rMet-treated NAFLD mice without a significant difference in food consumption, Metrnl overexpression indeed decreased TG accumulation in the FFA-treated HepG2 cells and mouse primary hepatocytes *in vitro*. In addition, body weight did not obviously differ between the LKO-Met and L-WT groups fed an HFD, but LKO-Met mice exhibited more severe hepatic steatosis than L-WT mice. Therefore, although the loss of body weight may contribute to the improvement in steatosis in rMet-treated mice, the alleviation of hepatic steatosis caused by Metrnl is still caused mainly by increased hepatic TG secretion.

Limitations of the study

In this study, we found that Metrnl mediated an increase in p-Akt levels through a PI3K p110 α -dependent pathway; however, the mechanisms by which Metrnl regulates the p110 α subunit to activate Akt require further investigation. We also showed that rMet treatment increased LDL activity and promoted FAO, but direct evidence is still needed to investigate whether the materials used in the FAO process in the liver and muscle originate from the TGs secreted by the liver. While Metrnl has been shown to be a ligand for the KIT receptor tyrosine kinase in endothelial cells, the specific receptor(s) of Metrnl that regulate lipid metabolism in hepatocytes and skeletal muscle cells remain to be identified. In addition, the functions of other lipid species regulated by Metrnl should be investigated further.

Our results provide evidence that Metrnl could be a potential therapeutic molecule for NAFLD. Metrnl promotes PC biosynthesis, leading to increased TG secretion, thus alleviating TG accumulation in hepatocytes. Additionally, we observed that Metrnl positively regulates FAO in the liver and skeletal muscle through an AMPK-dependent pathway. These results highlight the unexpected role of Metrnl in regulating hepatic lipid homeo-

stasis and have significant implications for the systemic regulation of TG levels.

RESOURCE AVAILABILITY

Lead contact

Requests for further information, resources, and reagents should be directed to and will be fulfilled by the lead contact, Guo Bing (guobingbs@126.com).

Materials availability

Plasmids and antibodies generated in this study will be shared by the [lead contact](#) upon request.

Data and code availability

- The accession number for the raw untargeted metabolomics data can be found in [STAR Methods](#).
- No new code was generated for this manuscript.
- All data reported in this paper will be shared by the [lead contact](#) upon ethics consideration and request.

ACKNOWLEDGMENTS

We are grateful to the National Natural Science Foundation of China (82060111, 82000741, 32160207, and 82170743), the Guizhou Youth Science and Technology Talent Support Program (GASTYESS202433), the Natural Science Foundation of Guizhou Provincial Education Department (Young Science and Technology Top-notch Talent Project) ([2024]328), and Guizhou Provincial Science and Technology Projects (ZK [2024]218). The Guizhou Provincial Natural Science Foundation ([2021]4029 and [2022]4017) supported this study.

AUTHOR CONTRIBUTIONS

Study concept and design, B.G., T.W., and M.S.; acquisition of data, Y.H., L.L., X.C., L.H., G.W., and H.Y.; experiment, L.S., Y.Z., T.Z., Y.W., and Y.X.; histological analysis, L.X.; funding collection, L.S., Y.Z., and B.G.; statistical analysis, S.R. and Q.S.; analysis and interpretation of data, L.S., Y.Z., and L.L.; drafting of the manuscript, L.S.; critical revision of the manuscript for important intellectual content, B.G., T.L., and M.S.

DECLARATION OF INTERESTS

The authors declare no competing interests.

STAR METHODS

Detailed methods are provided in the online version of this paper and include the following:

- [KEY RESOURCES TABLE](#)
- [EXPERIMENTAL MODEL AND STUDY PARTICIPANT DETAILS](#)
 - Patient samples
 - Animal studies
- [METHOD DETAILS](#)
 - Cell culture and treatments
 - Lipid sample preparation and lipidomic assay
 - Fractionation and FPLC
 - *In vivo* VLDL-TG secretion assay
 - Metrnl overexpression in *db/db* mice
 - Free fatty acid (FFA) preparation
 - Primary hepatocyte isolation
 - RNA *in situ* hybridization
 - Immunohistochemistry (IHC)
 - Immunofluorescence (IF) staining
 - RNA extraction, reverse transcription, and quantitative real-time PCR (qPCR)
 - Western blot analysis
 - Histological analysis

- ¹³C-labeled choline tracer studies
- Expression and purification of recombinant mouse Metrnl
- Serum, hepatic and cellular lipid measurements
- ELISA of Metrnl levels
- Seahorse analysis
- Dual-luciferase reporter assay
- Chromatin immunoprecipitation assay
- QUANTIFICATION AND STATISTICAL ANALYSIS

SUPPLEMENTAL INFORMATION

Supplemental information can be found online at <https://doi.org/10.1016/j.celrep.2025.115246>.

Received: October 2, 2024

Revised: November 29, 2024

Accepted: January 9, 2025

Published: February 5, 2025

REFERENCES

1. Fang, C., Pan, J., Qu, N., Lei, Y., Han, J., Zhang, J., and Han, D. (2022). The AMPK pathway in fatty liver disease. *Front. Physiol.* 13, 970292. <https://doi.org/10.3389/fphys.2022.970292>.
2. Zheng, Y., Qu, H., Xiong, X., Wang, Y., Liu, X., Zhang, L., Liao, X., Liao, Q., Sun, Z., Ouyang, Q., et al. (2019). Deficiency of Mitochondrial Glycerol 3-Phosphate Dehydrogenase Contributes to Hepatic Steatosis. *Hepatology* 70, 84–97. <https://doi.org/10.1002/hep.30507>.
3. Imai, N., and Cohen, D.E. (2018). Trimming the Fat: Acetyl-CoA Carboxylase Inhibition for the Management of NAFLD. *Hepatology* 68, 2062–2065. <https://doi.org/10.1002/hep.30206>.
4. Peng, Y., Zeng, Q., Wan, L., Ma, E., Li, H., Yang, X., Zhang, Y., Huang, L., Lin, H., Feng, J., et al. (2021). GP73 is a TBC-domain Rab GTPase-activating protein contributing to the pathogenesis of non-alcoholic fatty liver disease without obesity. *Nat. Commun.* 12, 7004. <https://doi.org/10.1038/s41467-021-27309-1>.
5. Fabbrini, E., Mohammed, B.S., Magkos, F., Korenblat, K.M., Patterson, B.W., and Klein, S. (2008). Alterations in adipose tissue and hepatic lipid kinetics in obese men and women with nonalcoholic fatty liver disease. *Gastroenterology* 134, 424–431. <https://doi.org/10.1053/j.gastro.2007.11.038>.
6. Quinn, W.J., 3rd, Wan, M., Shewale, S.V., Gelfer, R., Rader, D.J., Birnbaum, M.J., and Titchenell, P.M. (2017). mTORC1 stimulates phosphatidylcholine synthesis to promote triglyceride secretion. *J. Clin. Invest.* 127, 4207–4215. <https://doi.org/10.1172/jci96036>.
7. Metz, M., Beghini, M., Wolf, P., Pfleger, L., Hackl, M., Bastian, M., Freudenthaler, A., Harreiter, J., Zeyda, M., Baumgartner-Parzer, S., et al. (2022). Leptin increases hepatic triglyceride export via a vagal mechanism in humans. *Cell Metabol.* 34, 1719–1731.e5. <https://doi.org/10.1016/j.cmet.2022.09.020>.
8. Tardif, J.C., Karwatowska-Prokopczuk, E., Amour, E.S., Ballantyne, C.M., Shapiro, M.D., Moriarty, P.M., Baum, S.J., Hurh, E., Bartlett, V.J., Kingsbury, J., et al. (2022). Apolipoprotein C-III reduction in subjects with moderate hypertriglyceridaemia and at high cardiovascular risk. *Eur. Heart J.* 43, 1401–1412. <https://doi.org/10.1093/eurheartj/ehab820>.
9. Jung, T.W., Lee, S.H., Kim, H.C., Bang, J.S., Abd El-Aty, A.M., Hacimüftüoglu, A., Shin, Y.K., and Jeong, J.H. (2018). METRN attenuates lipid-induced inflammation and insulin resistance via AMPK or PPARδ-dependent pathways in skeletal muscle of mice. *Exp. Mol. Med.* 50, 1–11. <https://doi.org/10.1038/s12276-018-0147-5>.
10. Miao, Z.W., Hu, W.J., Li, Z.Y., and Miao, C.Y. (2020). Involvement of the secreted protein Metrnl in human diseases. *Acta Pharmacol. Sin.* 41, 1525–1530. <https://doi.org/10.1038/s41401-020-00529-9>.
11. Li, Z.Y., Song, J., Zheng, S.L., Fan, M.B., Guan, Y.F., Qu, Y., Xu, J., Wang, P., and Miao, C.Y. (2015). Adipocyte Metrnl Antagonizes Insulin Resistance Through PPARγ Signaling. *Diabetes* 64, 4011–4022. <https://doi.org/10.2337/db15-0274>.
12. Rao, R.R., Long, J.Z., White, J.P., Svensson, K.J., Lou, J., Lokurkar, I., Jendrychowski, M.P., Ruas, J.L., Wrann, C.D., Lo, J.C., et al. (2014). Meteorin-like is a hormone that regulates immune-adipose interactions to increase beige fat thermogenesis. *Cell* 157, 1279–1291. <https://doi.org/10.1016/j.cell.2014.03.065>.
13. Yao, Z.M., and Vance, D.E. (1988). The active synthesis of phosphatidylcholine is required for very low density lipoprotein secretion from rat hepatocytes. *J. Biol. Chem.* 263, 2998–3004.
14. Millar, J.S., Cromley, D.A., McCoy, M.G., Rader, D.J., and Billheimer, J.T. (2005). Determining hepatic triglyceride production in mice: comparison of poloxamer 407 with Triton WR-1339. *J. Lipid Res.* 46, 2023–2028. <https://doi.org/10.1194/jlr.D500019-JLR200>.
15. Vance, D.E. (2013). Physiological roles of phosphatidylethanolamine N-methyltransferase. *Biochim. Biophys. Acta* 1831, 626–632. <https://doi.org/10.1016/j.bbapap.2012.07.017>.
16. Niebergall, L.J., Jacobs, R.L., Chaba, T., and Vance, D.E. (2011). Phosphatidylcholine protects against steatosis in mice but not non-alcoholic steatohepatitis. *Biochim. Biophys. Acta* 1811, 1177–1185. <https://doi.org/10.1016/j.bbapap.2011.06.021>.
17. Ling, J., Chaba, T., Zhu, L.F., Jacobs, R.L., and Vance, D.E. (2012). Hepatic ratio of phosphatidylcholine to phosphatidylethanolamine predicts survival after partial hepatectomy in mice. *Hepatology* 55, 1094–1102. <https://doi.org/10.1002/hep.24782>.
18. Sugimoto, H., Banchio, C., and Vance, D.E. (2008). Transcriptional regulation of phosphatidylcholine biosynthesis. *Prog. Lipid Res.* 47, 204–220. <https://doi.org/10.1016/j.plipres.2008.01.002>.
19. Rebold, M.R., Klede, S., Taft, M.H., Cai, C.L., Field, L.J., Lavine, K.J., Koenig, A.L., Fleischauer, J., Meyer, J., Schambach, A., et al. (2022). Meteorin-like promotes heart repair through endothelial KIT receptor tyrosine kinase. *Science* 376, 1343–1347. <https://doi.org/10.1126/science.abn3027>.
20. Wang, Z.Q., Cai, Q., Hu, L., He, C.Y., Li, J.F., Quan, Z.W., Liu, B.Y., Li, C., and Zhu, Z.G. (2017). Long noncoding RNA UCA1 induced by SP1 promotes cell proliferation via recruiting EZH2 and activating AKT pathway in gastric cancer. *Cell Death Dis.* 8, e2839. <https://doi.org/10.1038/cddis.2017.143>.
21. Chen, Y., Tang, Q., Wu, J., Zheng, F., Yang, L., and Hann, S.S. (2015). Inactivation of PI3-K/Akt and reduction of SP1 and p65 expression increase the effect of solamargine on suppressing EP4 expression in human lung cancer cells. *J. Exp. Clin. Cancer Res.* 34, 154. <https://doi.org/10.1186/s13046-015-0272-0>.
22. Imai, N., Nicholls, H.T., Alves-Bezerra, M., Li, Y., Ivanova, A.A., Ortlund, E.A., and Cohen, D.E. (2022). Up-regulation of thioesterase superfamily member 2 in skeletal muscle promotes hepatic steatosis and insulin resistance in mice. *Hepatology* 75, 154–169. <https://doi.org/10.1002/hep.32122>.
23. Zhou, Y., Liu, L., Jin, B., Wu, Y., Xu, L., Chang, X., Hu, L., Wang, G., Huang, Y., Song, L., et al. (2023). Metrnl Alleviates Lipid Accumulation by Modulating Mitochondrial Homeostasis in Diabetic Nephropathy. *Diabetes* 72, 611–626. <https://doi.org/10.2337/db22-0680>.
24. Long, Y.C., and Zierath, J.R. (2006). AMP-activated protein kinase signaling in metabolic regulation. *J. Clin. Invest.* 116, 1776–1783. <https://doi.org/10.1172/jci29044>.
25. Davies, B.S.J., Beigneux, A.P., Barnes, R.H., 2nd, Tu, Y., Gin, P., Weinstein, M.M., Nobumori, C., Nyrén, R., Goldberg, I., Olivecrona, G., et al. (2010). GPIHBP1 is responsible for the entry of lipoprotein lipase into capillaries. *Cell Metabol.* 12, 42–52. <https://doi.org/10.1016/j.cmet.2010.04.016>.

26. Cole, L.K., Vance, J.E., and Vance, D.E. (2012). Phosphatidylcholine biosynthesis and lipoprotein metabolism. *Biochim. Biophys. Acta* 1821, 754–761. <https://doi.org/10.1016/j.bbapap.2011.09.009>.
27. Männistö, V., Kaminska, D., Kärjä, V., Tiainen, M., de Mello, V.D., Hanhineva, K., Soininen, P., Ala-Korpela, M., and Pihlajamäki, J. (2019). Total liver phosphatidylcholine content associates with non-alcoholic steatohepatitis and glycine N-methyltransferase expression. *Liver Int.* 39, 1895–1905. <https://doi.org/10.1111/liv.14174>.
28. Payne, F., Lim, K., Girousse, A., Brown, R.J., Kory, N., Robbins, A., Xue, Y., Sleigh, A., Cochran, E., Adams, C., et al. (2014). Mutations disrupting the Kennedy phosphatidylcholine pathway in humans with congenital lipodystrophy and fatty liver disease. *Proc. Natl. Acad. Sci. USA* 111, 8901–8906. <https://doi.org/10.1073/pnas.1408523111>.
29. Zhang, S., Huang, P., Dai, H., Li, Q., Hu, L., Peng, J., Jiang, S., Xu, Y., Wu, Z., Nie, H., et al. (2020). TIMELESS regulates sphingolipid metabolism and tumor cell growth through Sp1/ACER2/S1P axis in ER-positive breast cancer. *Cell Death Dis.* 11, 892. <https://doi.org/10.1038/s41419-020-03106-4>.
30. Saltiel, A.R., and Kahn, C.R. (2001). Insulin signalling and the regulation of glucose and lipid metabolism. *Nature* 414, 799–806. <https://doi.org/10.1038/414799a>.
31. Han, S., Liang, C.P., Westerterp, M., Senokuchi, T., Welch, C.L., Wang, Q., Matsumoto, M., Accili, D., and Tall, A.R. (2009). Hepatic insulin signaling regulates VLDL secretion and atherogenesis in mice. *J. Clin. Invest.* 119, 1029–1041. <https://doi.org/10.1172/jci36523>.
32. Yecies, J.L., Zhang, H.H., Menon, S., Liu, S., Yecies, D., Lipovsky, A.I., Gorgun, C., Kwiatkowski, D.J., Hotamisligil, G.S., Lee, C.H., and Manning, B.D. (2011). Akt stimulates hepatic SREBP1c and lipogenesis through parallel mTORC1-dependent and independent pathways. *Cell Metabol.* 14, 21–32. <https://doi.org/10.1016/j.cmet.2011.06.002>.
33. Bijl, N., Sokolović, M., Vrins, C., Langeveld, M., Moerland, P.D., Ottenhoff, R., van Roomen, C.P.A.A., Claessen, N., Boot, R.G., Aten, J., et al. (2009). Modulation of glycosphingolipid metabolism significantly improves hepatic insulin sensitivity and reverses hepatic steatosis in mice. *Hepatology* 50, 1431–1441. <https://doi.org/10.1002/hep.23175>.
34. Sopasakis, V.R., Liu, P., Suzuki, R., Kondo, T., Winnay, J., Tran, T.T., Asano, T., Smyth, G., Sajan, M.P., Farese, R.V., et al. (2010). Specific roles of the p110alpha isoform of phosphatidylinsitol 3-kinase in hepatic insulin signaling and metabolic regulation. *Cell Metabol.* 11, 220–230. <https://doi.org/10.1016/j.cmet.2010.02.002>.
35. Jackson, L.N., Larson, S.D., Silva, S.R., Rychahou, P.G., Chen, L.A., Qiu, S., Rajaraman, S., and Evers, B.M. (2008). PI3K/Akt activation is critical for early hepatic regeneration after partial hepatectomy. *Am. J. Physiol. Gastrointest. Liver Physiol.* 294, G1401–G1410. <https://doi.org/10.1152/ajpgi.00062.2008>.
36. Cornell, R.B., and Ridgway, N.D. (2015). CTP:phosphocholine cytidylyltransferase: Function, regulation, and structure of an amphitropic enzyme required for membrane biogenesis. *Prog. Lipid Res.* 59, 147–171. <https://doi.org/10.1016/j.plipres.2015.07.001>.
37. Qi, Q., Hu, W.J., Zheng, S.L., Zhang, S.L., Le, Y.Y., Li, Z.Y., and Miao, C.Y. (2020). Metnrl deficiency decreases blood HDL cholesterol and increases blood triglyceride. *Acta Pharmacol. Sin.* 41, 1568–1575. <https://doi.org/10.1038/s41401-020-0368-8>.
38. Minokoshi, Y., Kim, Y.B., Peroni, O.D., Fryer, L.G.D., Müller, C., Carling, D., and Kahn, B.B. (2002). Leptin stimulates fatty-acid oxidation by activating AMP-activated protein kinase. *Nature* 415, 339–343. <https://doi.org/10.1038/415339a>.
39. Woods, A., Johnstone, S.R., Dickerson, K., Leiper, F.C., Fryer, L.G.D., Neumann, D., Schlattner, U., Wallmann, T., Carlson, M., and Carling, D. (2003). LKB1 is the upstream kinase in the AMP-activated protein kinase cascade. *Curr. Biol.* 13, 2004–2008. <https://doi.org/10.1016/j.cub.2003.10.031>.
40. Woods, A., Dickerson, K., Heath, R., Hong, S.P., Momcilovic, M., Johnstone, S.R., Carlson, M., and Carling, D. (2005). Ca2+/calmodulin-dependent protein kinase kinase-beta acts upstream of AMP-activated protein kinase in mammalian cells. *Cell Metabol.* 2, 21–33. <https://doi.org/10.1016/j.cmet.2005.06.005>.
41. Antonia, R.J., and Baldwin, A.S. (2018). IKK promotes cytokine-induced and cancer-associated AMPK activity and attenuates phenformin-induced cell death in LKB1-deficient cells. *Sci. Signal.* 11, eaan5850. <https://doi.org/10.1126/scisignal.aan5850>.
42. Li, C., Dong, X., Du, W., Shi, X., Chen, K., Zhang, W., and Gao, M. (2020). LKB1-AMPK axis negatively regulates ferroptosis by inhibiting fatty acid synthesis. *Signal Transduct. Targeted Ther.* 5, 187. <https://doi.org/10.1038/s41392-020-00297-2>.

STAR★METHODS

KEY RESOURCES TABLE

REAGENT or RESOURCE	SOURCE	IDENTIFIER
Antibodies		
anti-Metnrl	Sigma-Aldrich	Cat#: HPA023792; RRID:AB_2144182
anti-Metnrl	R&D	Cat#: MAB6679; RRID:AB_3658642
anti-Metnrl	Abcam	RRID: ab235775;
anti-Metnrl for neutralization	R&D	Cat#: AF6679 ^[12] ; RRID:AB_10971292
anti-F4/80	Proteintech	Cat#: 29414-1-AP; RRID:AB_2918300
anti-GAPDH	Proteintech	Cat#: 60004-1; RRID:AB_2107436
anti- α -tubulin	Proteintech	Cat#: 11224-1-AP; RRID:AB_2210206
anti-CHKA	Cell Signaling Technology	RRID: 13422S
anti-CCT α	Cell Signaling Technology	RRID: 6931S
anti- p -Akt ^{Ser473}	Cell Signaling Technology	Cat#: 4060; RRID:AB_2315049
anti-Akt	Proteintech	Cat#: 60203-2-Ig; RRID:AB_10912803
anti- p -AMPK ^{Thr172}	Cell Signaling Technology	Cat#: D4D6D; RRID:AB_2799368
anti-AMPK	Proteintech	Cat#: 10929-2-AP; RRID:AB_2169568
anti-CPT1A	Proteintech	Cat#: 15184-1-AP; RRID:AB_2084676
anti-Sp1	Proteintech	Cat#: 21962-1-AP; RRID:AB_10898171
anti-HA Tag	Thermo Fisher	Cat#: RM305; RRID:AB_2744968
anti- p -LKB1	Cell Signaling Technology	RRID: 3482S
anti- p -CamKK2	Cell Signaling Technology	RRID: 35392S
anti- p -TAK1	Cell Signaling Technology	RRID: 4508S
anti-FASN	Santa Cruz	Cat#: sc-48357; RRID:AB_627584
anti-SREBP1	Abcam	Cat#: ab28481; RRID:AB_778069
Goat anti-rabbit IgG(H + L), HRP	ZSGB-BIO	Cat#: ZB2301; RRID:AB_2747412
Goat anti-Mouse IgG(H + L), HRP	ZSGB-BIO	Cat#: ZB5305; RRID:AB_2923203
Bacterial and virus strains		
DH5 α competent cells	Invitrogen	Cat#:18265017
Biological samples		
Human tissue arrays	Bioaitech Co.,Ltd.	Cat#DP067Lv01
Chemicals, peptides, and recombinant proteins		
Endotoxin-free mouse recombinant protein Metnrl	AtaGenix	Zhou et al. ^[23]
PMSF	MedChemExpress	Cat#: HY-B0496
Percoll	Solarbio	Cat#: P0100
DTT	Sigma-Aldrich	Cat#: 10197777001
Phosphatase Inhibitor Cocktail	MedChemExpress	Cat#: HY-K0022
Protease Inhibitor Cocktail	MedChemExpress	Cat#: HY-K0010
TRIzol	Invitrogen	Cat#: 15596026
Palmitate	Sigma-Aldrich	Cat#: P5585
Oleic acid	Aladdin	Cat#: O108487
Biotin-Streptavidin HRP Detection Systems	ZSGB-BIO	Cat#: SP-9000
Haematoxylin Eosin Staining Assay Kit	PHYGENE	Cat#: PH0516
ECL Prime Western Blotting Detection Reagent	Smart-Lifesciences	Cat#: RPN2232SK

(Continued on next page)

Continued

REAGENT or RESOURCE	SOURCE	IDENTIFIER
DEPC	Beyotime	Cat#: R0021
Fatty acid-free BSA	MPBio	Cat#: 219989980
Collagenase IV	Sigma-Aldrich	Cat#: C4-22
Mithramycin	MedChemExpress	Cat#: HY-A0122
LY294002	Cell Signaling Technology	Cat#: 9901S
PIK75	MedChemExpress	Cat#: HY-107834
TGX221	MedChemExpress	Cat#: HY-10114
CDP-choline	Sigma-Aldrich	Cat#: 30290
Rat tail tendon collagen type I	Solarbio	Cat#: C8065
1,2- ¹³ C choline	Cambridge Isotopes	Cat#: CLM-548-0.1
Poloxamer 407	MedChemExpress	Cat#: HY-D1005
Critical commercial assays		
Dual-Luciferase TM Reporter (DLR TM) Assay System	Promega	Cat#: E1960
SYBR [®] Premix Ex Taq [™] II	Takara	Cat#: RR820A
PrimeScript TM RT reagent Kit withgDNA Eraser	Takara	Cat#: RR047A
AST Assay Kit	Nanjing Jiancheng Bioengineering Institute	Cat#: C10-2-1
ALT Assay Kit	Nanjing Jiancheng Bioengineering Institute	Cat#: C009-1-1
Human Meteorin-like/METRNL DuoSet ELISA	R&D	Cat#: DY7867-05
Substrate Reagent Pack	R&D	Cat#: DY999
DuoSet ELISA Ancillary Reagent Kit 2	R&D	Cat#: DY008
Phosphatidylcholine Colorimetric Assay Kit	Cayman	Cat#: 10009926
Enhanced ATP Assay Kit	Beyotime	Cat#: S0027
TIANGel Purification Kit	TIANGEN	Cat#: DP219
EndoFree Mini Plasmid Kit II	TIANGEN	Cat#: DP118-02
β-Hydroxybutyrate (Ketone Body) Colorimetric Assay Kit	Cayman	Cat#: CAY-700190-96
Seahorse XFp Cell Mito Stress Test Kit	Agilent	Cat#: 103017-100
SimpleChIP [®] Enzymatic Chromatin IP Kit (Magnetic Beads)	Cell Signaling Technology	Cat#: 9003
Deposited data		
Lipidomics –Figure 3	This paper	OMIX: 008005
Experimental models: Cell lines		
Human embryonic kidney 293T (HEK293T) cells	CELL RESEARCH	Cat#: ZQ0033
Mouse hepatocytes (AML12)	CELL RESEARCH	Cat#: ZQ0303
Human hepatocellular carcinoma cell line (HepG2)	National Collection of Authenticated Cell Cultures	Cat#: SCSP-510
C2C12 mouse myoblasts	CELL RESEARCH	Cat#: ZQ1116
Experimental models: Organisms/strains		
C57BL/6J	SPF (Beijing) Biotechnology Co.,Ltd.	https://www.spfbiotech.com/
C57BL/6JGpt-Lepri ^{em2Cd3571} /Gpt	GemPharmatech	https://www.gempharmatech.com/index.html
C57BL/6JGpt-Metnrl ^{fl/fl}	GemPharmatech	https://www.gempharmatech.com/index.html
C57BL/6JGpt-Alb-Cre	Cyagen	https://www.cyagen.com/us/en/

(Continued on next page)

Continued

REAGENT or RESOURCE	SOURCE	IDENTIFIER
Oligonucleotides		
<i>Homo Metnl</i> AGTGGATGTACCCAACAGGTG TACCAGCAGTCTCAGTTCTCC	Sangon Biotech	N/A
<i>Homo Gapdh</i> TGCACCACCAACTGCTTAG GGATGCAGGGATGATGTTC	Sangon Biotech	N/A
<i>Homo Pcyt1α</i> TTTGCTCCAACACAGAGGACAGAAG GGTTCGCCCTCGCATACACATC	Sangon Biotech	N/A
<i>Homo Chka</i> ACCCTTGGTATGAGCCTCG GCTCTCAGAACCATGGCCT	Sangon Biotech	N/A
<i>Homo Cept</i> TTTGCTGGCAGTGATTGGAGGAC ACCACCTGTGAAGATTACACGGAAAG	Sangon Biotech	N/A
<i>Homo Cd36</i> GGAAGTGATGATGAACAGCAGCAAC TGTCCCTAGCGTCCTGGTTAC	Sangon Biotech	N/A
<i>Homo Fatp1</i> ACCGCATATAACCAGGAGCTG ATCTGAAGGTGCCTGTGGT	Sangon Biotech	N/A
<i>Homo Srebf1</i> GCTGTTGGTGCCTCGTCCTTG GCTTGCATGCCTCCAGAAGTAC	Sangon Biotech	N/A
<i>Homo Pparg</i> CATAAGTCCTCCCCGCTGA TCTGTGATCCTGCACAGC	Sangon Biotech	N/A
<i>Homo Cpt1a</i> GCACATCGTCGTGTACCATC AATAGGCCTGACGACACCTG	Sangon Biotech	N/A
<i>Homo Mtp</i> CTTCTGGCCTTCATTCA AGCAGAGGTGACAGCATCCA	Sangon Biotech	N/A
<i>Homo ApoB</i> TACTGGACGAACCTGGCTGACC GGCTTCTCAACGGCATCTCAT	Sangon Biotech	N/A
<i>Homo PEMT</i> AACACAAGACCCGAAAGCTGAG GCAGGAAGTTCAGGAGCAGGATG	Sangon Biotech	N/A
<i>Mus Metnl</i> GGAATTCCCTTCACTGGACAT CTTCTGCTTCTGTACATCCT	Sangon Biotech	N/A
<i>Mus Gapdh</i> AGGTCGGTGTGAACGGATTG TGTAGACCATGTAGTTGAGGTCA	Sangon Biotech	N/A
<i>Mus Pcyt1α</i> GCCTGTGAGAGTTATGCGGATG AAGCCCTGAAGTTGCGTTAG	Sangon Biotech	N/A
Primer 1 for CHIP: CCCAAACATGGTTTGTGGGG TTCATGCCAACATCGCGTC	Sangon Biotech	N/A
Primer 2 for CHIP: TGCCTTATTCTACCGCGGTG TTAAGTCCGGGGTCAAAGGC	Sangon Biotech	N/A
Primer 3 for CHIP: GACTGTGACGGAAGTGAGGC ACTTCCGTTCTCGCGTTCG	Sangon Biotech	N/A

(Continued on next page)

Continued

REAGENT or RESOURCE	SOURCE	IDENTIFIER
Primer 4 for CHIP: ACTGTGACGGAAGTGAGGCT CTTCGGCCCTTCCAT	Sangon Biotech	N/A
Primer 5 for CHIP: CTTTCTGCGGAGGTAAAGGAGA ATCCGCTCCAAAACGGTA	Sangon Biotech	N/A
Primer 6 for CHIP: GTCTCAAAACCCCTGCCGC CTCCTTACCTCCGCAGAAA	Sangon Biotech	N/A
shRNA-Metrln: CAAGGACTTCCAGAGGATGT	N/A	N/A
Recombinant DNA		
AAV8-Metrln	HANBIO	N/A
AAV8-Vector	HANBIO	N/A
Ad-mouse Metrln	OBio Technology Corp.Ltd	N/A
Ad-mouse Vector	OBio Technology Corp.Ltd	N/A
Ad-human Metrln	OBio Technology Corp.Ltd	N/A
Ad-human Vector	OBio Technology Corp.Ltd	N/A
pGL3-CCT α -promotor	This paper	N/A
pGL3	This paper	N/A
sh-Metrln	OBio Technology Corp.Ltd	N/A
sh-Vector	OBio Technology Corp.Ltd	N/A
Software and algorithms		
GraphPad Prism 9.03	GraphPad Software	https://www.graphpad.com/features
EndNote X8	EndNote	https://endnote.com/
Adobe Illustrator	Adobe	https://www.adobe.com/
ImageJ	NIH	https://imagej.net/ij/
Adobe Photoshop	Adobe	https://www.adobe.com/
Other		
Ethical approval of the human tissue array	Life Sciences Ethics Committee of Changsha Yaxiang Biotechnology Co., LTD.	Csyayj2024093

EXPERIMENTAL MODEL AND STUDY PARTICIPANT DETAILS

Patient samples

All liver tissue arrays used in this study were purchased from Bioaitech Co., Ltd. (Xi'an, China). The normal tissues used in Figure S1A, healthy human liver tissues ($n = 11$) and NAFLD liver tissues ($n = 9$) were obtained from tumor-adjacent tissues of individuals with hepatic carcinoma who were diagnosed with NAFLD after surgery.

Animal studies

Eight-week-old male C57BL/6 mice were from SPF (Beijing) Biotechnology Co.,Ltd., 10-week-old male *db/m* mice and *db/db* mice were purchased from Gempharmatech Co., Ltd. After a 2-week acclimation period, the C57BL/6 mice were randomly divided into the corresponding experimental groups and fed an HFD for 12 or 16 weeks to induce hepatic steatosis. At 12 weeks of age, C57BL/6 mice were fed a choline and methionine-deficient (MCD) diet or a choline and methionine-supplemented (MCS) diet for 6 weeks, accompanied by rMet injections. For the experiments using the recombinant protein, rMet (0.3 mg/kg body weight) or a saline solution was administered via intravenous injection into the tail vein every other day for the specified duration.

Metrln-floxed (*Metrln*^{flox/flox}) mice were obtained from GemPharmatech Co., Ltd., and Alb-Cre (Alb-Cre) recombinase transgenic mice were obtained from Cyagen. *Metrln*^{flox/flox} mice were crossed with Alb-Cre mice to generate hepatocyte-specific *Metrln*-deficient mice (LKO-Met, *Metrln*^{flox/flox}, *Alb-Cre*⁺). Littermates of *Metrln*^{flox/flox}, *Alb-Cre*⁻ (L-WT) mice were used as the control group. All the animals used in this study were healthy and vibrant, and their initial body weights differed by less than 2 g. The mice were housed in a temperature-controlled room with a 12 h:12 h light:dark cycle. At the end of each experiment, the animals were sacrificed after being

anesthetized. The experimental protocol was approved by the Guizhou Medical University Institutional Animal Ethics Committee (No. 2000639).

METHOD DETAILS

Cell culture and treatments

Human HepG2 and AML12 cells were obtained from CELL RESEARCH (Shanghai, China). HepG2 cells were cultured in DMEM (Gibco, 4.5 g/L glucose) containing 10% FBS, and AML12 cells were cultured in DMEM/F12 containing 10% FBS, 1× insulin–transferrin–selenium supplement and dexamethasone (40 ng/mL). For the high-fat treatment, HepG2 and AML12 cells were exposed to 0.3 mmol/L FFAs (palmitic acid:oil acid = 1:2) containing 10% BSA for the indicated durations, and 10% BSA was used as a control.

For adenoviral vector transfection, the vectors used for Metrnl overexpression and knockdown were obtained from OBiO Technology Corp., Ltd. (Shanghai, China). Recombinant adenoviruses were generated using the AdEasy Adenovirus System. Briefly, the Metrnl gene was cloned and inserted into the pAdTrack-CMV vector. The linearized plasmid was then transformed into AdEasier cells to generate recombinant adenoviral plasmids, which were subsequently transfected into 293A cells to obtain the recombinant adenovirus (referred to as Ad-Met below). For lentivirus-mediated gene knockdown, shRNA-Metrnl (sh-Met) was cloned and inserted into a vector containing an HA tag. The recombinant virus was prepared using the same method as described above.

Lipid sample preparation and lipidomic assay

For the untargeted lipidomic analysis, lipids were extracted from the liver tissues using the MTBE method and redissolved in 90% isopropanol. The extracts were then analyzed using ultra-performance liquid chromatography and a Q Exactive plus mass spectrometer (Thermo Scientific) at Applied Protein Technology Co., Ltd. (Shanghai, China).

Fractionation and FPLC

The serum lipoprotein distribution in the VLDL, LDL, and HDL fractions was determined using fast protein–liquid chromatography (FPLC) fractionation on a Labospect 008AS automatic biochemical analyzer (HITACHI). Equal volumes (200 µL) of pooled serum samples from each group (5 mice per group) were used for detection.

In vivo VLDL-TG secretion assay

Hepatic VLDL-TG secretion was measured by inhibiting VLDL catabolism with poloxamer 407.⁶ For detail, the mice were subjected to a 6-h period of starvation, followed by an intraperitoneal injection of poloxamer 407 (1 mg/g body weight). Blood samples were collected from the tail vein at specified time points after the injection and utilized for TG detection.

Metrnl overexpression in db/db mice

The delivery vector construction, viral packaging, and titration of adeno-associated virus 8 expressing Metrnl (AAV8-Metrnl) and the control (AAV8-Vector) were performed by HANBIO. Twelve-week-old male db/db mice were intravenously injected with 5 × 10¹¹ pfu of the virus, and tissues and serum were harvested for detection after 16 weeks.

Free fatty acid (FFA) preparation

The 100 mM palmitate (Sigma, USA) and 100 mM oleic acid (Aladdin, China) stock solutions were prepared in 0.1 mmol/L NaOH or absolute ethanol, respectively, and filtered through a 0.22 mm filter. A 10% mass volume of a fatty acid-free BSA (MPBio, USA) solution was prepared, and an FFA solution (palmitate:oleate at a 1:2 ratio) was added to 10% BSA to prepare a 5 mM free fatty acid-BSA solution.

Primary hepatocyte isolation

Primary hepatocytes were isolated from 6- to 8-week-old mice via liver perfusion. The L-WT and LKO-Met mice were anesthetized with isoflurane. D-Hank's buffer salt solution (Solarbio, China) was perfused through the inferior vena cava, followed by D-Hank's buffer salt solution containing 0.05% collagenase IV (Sigma) for digestion. The resulting suspension was filtered through a 100 µm filter and washed 3 times with Hank's buffer. The cells were purified using a 90% Percoll solution (Cytiva, China). Cell viability was assessed via Trypan blue staining. The isolated primary hepatocytes were seeded in rat tail tendon collagen type I (Solarbio, China)-coated plates, cultured with Dulbecco's modified Eagle's medium, treated with 0.3 mM FFAs for 24 h to establish a NAFLD cell model, and used for further experiments.

RNA *in situ* hybridization

Metrnl mRNA expression in the liver was detected using a FISH detection kit (GenePharma, China) according to the manufacturer's instructions. Briefly, liver tissue arrays were deparaffinized and incubated with H₂O₂ to expose the RNA. The arrays were then immersed in Target Reagent solution and treated with Protease Plus. The liver tissue arrays were incubated with a human Metrnl probe mixture at 42°C overnight in a dark room. After DAPI staining, images were captured using an Olympus confocal microscope.

Immunohistochemistry (IHC)

Immunohistochemical staining was performed on paraformaldehyde-fixed tissues that were embedded in paraffin and sliced into 3 μm -thick sections. The sections were subjected to antigen retrieval using a sodium citrate solution, followed by blocking with 3% H₂O₂. The sections were then incubated overnight at 4°C with the indicated primary antibodies against Metnrl (R&D; Abcam) and Sp1 (Proteintech). After washes with PBS, the sections were treated with a secondary antibody and subjected to IHC staining. Finally, images were captured using an Olympus upright microscope.

Immunofluorescence (IF) staining

Liver tissues were fixed with 4% paraformaldehyde for 20 min, permeabilized with 0.2% Triton X-100 for 10 min, and blocked with 5% bovine serum albumin (Servicebio, China) for 40 min. The tissues were subsequently exposed to specific primary antibodies and incubated at 4°C overnight. FITC-conjugated goat anti-rabbit IgG served as the secondary antibody, and DAPI (Sigma, USA) was used for nuclear staining. The images were captured with an Olympus laser confocal microscope.

RNA extraction, reverse transcription, and quantitative real-time PCR (qPCR)

Total RNA was extracted from tissues and cells using TRIzol reagent. Reverse transcription was performed using the PrimeScript RT Reagent Kit with gDNA Eraser (Takara, Japan). The qPCR analysis was performed using SYBR Premix Ex Taq II (Takara, Japan). The expression levels of the target genes were calculated relative to those of GAPDH using the $2^{-\Delta\Delta\text{CT}}$ method. Each experiment was conducted in triplicate.

Western blot analysis

The cells and tissues were lysed in RIPA buffer containing PMSF, protease inhibitors and phosphatase inhibitors. The proteins were then denatured and subjected to SDS-PAGE. Nuclear proteins were collected using a nuclear protein extraction kit (Invent, China). The proteins were subsequently transferred to PVDF membranes and incubated with primary antibodies against GAPDH, Metnrl, CCT α , CHKA, Sp1, phospho-Akt^(Ser473), Akt, phospho-AMPK^(Thr172), AMPK (Proteintech), CPT1A, phospho-LKB1^(Ser428), phospho-CaMKK2^(Ser495), and phospho-TAK1^(Thr184/187) overnight at 4°C. The membranes were washed before an incubation with HRP-conjugated secondary antibodies for 2 h at room temperature. The signals were visualized using ECL detection reagents (Smart Life Sciences). The experiments were performed in triplicate.

Histological analysis

Paraffin sections of the liver tissue were stained with hematoxylin and eosin (H&E), and the area of hepatic steatosis and the infiltration of inflammatory cells were evaluated by three different pathologists. Frozen liver sections were subjected to Oil Red O staining to evaluate lipid accumulation in the liver. Histological images of the liver sections were captured using an upright microscope (Olympus, Japan), and the average staining intensity from five random fields (40 \times) was measured using Image-Pro Plus software to evaluate the protein expression levels in the liver sections.

¹³C-labeled choline tracer studies

AML12 cells were cultured, infected with adenovirus an to induce the expression of Metnrl (Ad-Met) or the control vector (Ad-Vec), and treated FFAs for 24 h. Then, the culture medium was removed and replaced with medium containing 1,2-¹³C choline together with the respective treatments for an additional 24 h. The 1,2-¹³C choline medium was prepared with DMEM without choline (Life Technologies) supplemented with 0.0286 mM 1,2-¹³C choline (Cambridge Isotopes, CLM-548-0.1). Then, 200 μL of extraction solution (80% methanol containing an internal standard mixture) was added to the cell pellet, and the cell pellet was lysed using an ultrasonic homogenizer (on dry ice). Then, 800 μL of extraction solution was added, and the mixture was vortexed for 1 min. After centrifugation at 14,000 $\times g$ at 4°C for 10 min, the supernatant was transferred to a new centrifuge tube and dried using a SpeedVac. The residue was redissolved in 100 μL of a 50% water/50% methanol solution, vortexed and centrifuged. The supernatant was used for mass spectrometry analysis.

Expression and purification of recombinant mouse Metnrl

The recombinant mouse Metnrl sequence used in this study was obtained from AtaGenix Laboratories Co., Ltd. (Wuhan, China). The cDNA fragment encoding mouse Metnrl was cloned and inserted into the expression vector pET-28b and transformed into the *E. coli* BL21 strain. The transformed *E. coli* BL21 strain was incubated with isopropyl- β -D-1-thiogalactopyranoside at 37°C for 18–20 h to induce the expression of the mouse Metnrl protein. The Metnrl protein was purified using heparin-affinity chromatography and size-exclusion chromatography with a Superdex-100 column.

Serum, hepatic and cellular lipid measurements

The TG contents in the serum, liver tissue, HepG2 cells, primary hepatocytes, and the indicated culture supernatants were measured using a TG assay kit (Applygen, China). PC and β -hydroxybutyrate contents were assessed using their respective assay kits (Cayman, USA). Serum ALT, AST, and LPL activities and HDL and TC contents were measured using assay kits (Nanjing Jiancheng Bioengineering Institute, China). The experiments were performed in triplicate.

For the analysis of TG secretion *in vitro*, the cells were treated with 0.3 mmol/L FFAs for 24 h, after which the medium was replaced with FBS- and phenol-free medium. After an additional 5 h of incubation, the medium was harvested, and the TG content in the medium was detected using a TG assay kit. For the detection of TG, PC and β -hydroxybutyrate levels in hepatocytes, the cells were treated with FFAs. After 24 h of incubation, the cells were lysed, and the TG, PC, and β -hydroxybutyrate contents were measured.

ELISA of Metrnl levels

The Human Metrnl ELISA Kit was purchased from R&D Systems. A total of 100 μ L of each sample was used for the analysis, and the assay was performed according to the protocol. The experiments were performed in triplicate.

Seahorse analysis

In accordance with the manufacturer's instructions, the Seahorse XFp Cell Mito Stress Test Kit (Agilent, USA) was used to measure the oxygen consumption levels in the cells treated with FFAs. The Seahorse XF Extracellular Flux Bioanalyzer was then used to analyze and measure the oxygen consumption rate (OCR). The experiments were performed in triplicate.

Dual-luciferase reporter assay

The plasmid was constructed by Hejin Bio. According to the JASPAR prediction, Sp1 binding sites are present in the CCT α promoter region. We constructed a plasmid containing the CCT α promoter region. Twenty-four hours after transfection, the firefly and Renilla luciferase activities were measured in 293T cells using the dual-luciferase reporter system (Promega, USA). The reporter activity was normalized to that of Renilla luciferase. The experiments were performed in triplicate.

Chromatin immunoprecipitation assay

Chromatin immunoprecipitation (ChIP) was performed using a kit from Cell Signaling Technology. Briefly, the DNA–protein complexes were crosslinked with 1% formaldehyde for 15 min. The crosslinked chromatin samples were isolated via nuclease digestion. Sp1 was immunoprecipitated using an anti-Sp1 or IgG antibody, after which the DNA was extracted. The DNA was amplified by qPCR with primers targeting the CCT α promoter, which contains the binding sites for Sp1 and CCT α . The primers for the CCT α promoter are presented in Table S1. The experiments were performed in triplicate.

QUANTIFICATION AND STATISTICAL ANALYSIS

The data are reported as the means \pm standard deviations (SDs) and were analyzed with GraphPad Prism. For normally distributed data, statistically significant differences between two groups and multiple groups were analyzed using Student's *t* tests and one-way ANOVA, respectively. For comparisons at multiple time points, two-way ANOVA followed by Dunnett's test were used. For data with a nonnormal distribution, the statistical significance of differences between two groups and multiple groups was analyzed using the Mann–Whitney test and the Kruskal–Wallis test, respectively. Fluorescence and protein band intensities were quantified using ImageJ software. In this study, ns represents no statistical significance; the value of *n* is labeled in each figure legend, and the *n* represents the number of animals; a *p*-value of less than 0.05 was considered statistically significant.